HHS Public Access

Author manuscript

Cell Host Microbe. Author manuscript; available in PMC 2018 July 12.

Published in final edited form as:

Cell Host Microbe. 2017 July 12; 22(1): 74–85.e7. doi:10.1016/j.chom.2017.06.005.

Viral replication complexes are targeted by LC3-guided interferon-inducible GTPases

Scott B. Biering[1,10], **Jayoung Choi**[2,10], **Rachel A. Halstrom**[2], **Hailey M. Brown**[3], **Wandy L. Beatty**[5], **Sanghyun Lee**[6], **Broc T. McCune**[6], **Erin Dominici**[2], **Lelia E. Williams**[4], **Robert C. Orchard**[6], **Craig B. Wilen**[6], **Masahiro Yamamoto**[7], **Jörn Coers**[8], **Gregory A. Taylor**[8,9], and **Seungmin Hwang**[1,2,3,*]

[1]Committee on Microbiology, The University of Chicago, Chicago, IL 60637, USA

[2]Department of Pathology, The University of Chicago, Chicago, IL 60637, USA

[3]Committee on Immunology, The University of Chicago, Chicago, IL 60637, USA

[4]Biological Sciences Collegiate Division, The University of Chicago, Chicago, IL 60637, USA

[5]Department of Molecular Microbiology, Washington University School of Medicine, St. Louis, MO 63110, USA

[6]Department of Pathology and Immunology, Washington University School of Medicine, St. Louis, MO 63110, USA

[7]Laboratory of Immunoparasitology, World Premier International Research Center Immunology Frontier Research Center, Osaka University, Osaka 565-0871, Japan

[8]Departments of Medicine, Molecular Genetics and Microbiology, and Immunology, Duke University Medical Center, Durham, NC 27710, USA

[9]GRECC, Durham VA Health Care System, Durham, NC 27705, USA

SUMMARY

All viruses with positive-sense RNA genomes replicate on membranous structures in the cytoplasm, called replication complexes (RCs). RCs provide an advantageous microenvironment for viral replication, but it is unknown how the host immune system counteracts these structures. Here we show that interferon-gamma (IFNG) disrupts the RC of murine norovirus (MNV) via evolutionarily conserved autophagy proteins and the induction of IFN-inducible GTPases, which are known to destroy the membrane of vacuoles containing bacteria, protists, or fungi. The MNV RC was marked by the microtubule-associated-protein-1-light-chain-3 (LC3) conjugation system of autophagy and then targeted by immunity-related GTPases (IRGs) and guanylate binding

*Correspondence to and Lead Contact: Seungmin Hwang; shwang@bsd.uchicago.edu.
[10]These authors contributed equally.

AUTHOR CONTRIBUTION

Conceptualization, S.B.B., J.C., and S.H.; Methodology, S.B.B., J.C., W.L.B., S.L., B.T.M., and S.H.; Investigation, S.B.B., J.C., R.A.H., H.M.B., W.L.B., S.L., B.T.M., E.D., L.E.W., and S.H.; Resources, R.C.O., C.B.W., M.Y., J.C., and G.A.T.; Writing – Original Draft, S.B.B. and S.H.; Writing – Review & Editing, S.B.B., J.C., G.A.T., S.H.; Visualization, S.B.B., J.C., and S.H.; Supervision, S.H.; Funding Acquisition, S.H.

All authors declare no conflict of interest.

proteins (GBPs) upon their induction by IFNG. Further, the LC3 conjugation system and the IFN-inducible GTPases were necessary to inhibit MNV replication in mice and human cells. These data suggest that viral RCs can be marked and antagonized by a universal immune defense mechanism targeting diverse pathogens replicating in cytosolic membrane structures.

Keywords

autophagy; ATG; LC3; targeting by autophagy proteins; interferon; IFN; interferon-inducible GTPase; immunity-related GTPase; IRG; guanylate binding protein; GBP; positive-sense RNA virus; replication complex; norovirus; vacuolar pathogen

INTRODUCTION

Positive-sense RNA (+RNA) viruses encompass about one-third of all known viruses, including many clinically relevant viruses (Boon et al., 2010). A hallmark of all known +RNA viruses is to rearrange host endomembranes to form vacuole-like structures in the cytoplasm for their replication, termed the replication complex (RC) (Boon et al., 2010). The RC provides +RNA viruses a base to exploit the cell and a shelter from the host immune system (Neufeldt et al., 2016; Shulla and Randall, 2016). However, it has been unclear how the host immune system counteracts viral RCs.

Recently, we found that the replication of murine norovirus (MNV) is inhibited by type II interferon (IFN), IFN-gamma (IFNG), at the stage of RC formation (Hwang et al., 2012) in contrast to type I IFNs that primarily inhibit the translation of MNV proteins (Changotra et al., 2009). Intriguingly, this antiviral activity of IFNG against the MNV RC depends on a protein complex involved in autophagy (Hwang et al., 2012). Autophagy is an evolutionarily conserved cellular pathway that delivers cytoplasmic material to lysosomes for degradation (Levine et al., 2011). Among the multiple types of autophagy, macroautophagy (henceforth, autophagy) is the major process that sequesters and transports cytosolic material inside double-membraned autophagosomes (Noda and Inagaki, 2015). For efficient formation of autophagosomes and selective capture of cargo, ubiquitin-like microtubule-associated-protein-1-light-chain-3 (LC3) and its homologs must be conjugated to the membrane-embedded lipid phosphatidylethanolamine (PE). Similar to the conjugation of ubiquitin to a target amino acid residue, an E1-like activating enzyme, ATG7, and an E2-like conjugating enzyme, ATG3, function together with an E3-like ligase, the ATG12-ATG5-ATG16L1 complex to conjugate LC3 to PE (Noda and Inagaki, 2015). We found that IFNG requires this E3-like ATG12-ATG5-ATG16L1 ligase complex but not lysosomal degradation through autophagy to inhibit MNV RC formation and viral replication (Hwang et al., 2012). However, it remains unknown how IFNG utilizes this E3-like ligase complex to inhibit the MNV RC.

Intriguingly, *Atg5* is also required for IFNG to inhibit the replication of a protist parasite *Toxoplasma gondii* (Zhao et al., 2008). *T. gondii* invades and replicates within a parasitophorus vacuole (PV); when cells are primed with IFNG, the PV membrane (PVM) is disrupted by IFN-inducible GTPases, immunity-related GTPases (IRGs) and guanylate binding proteins (GBPs) (Pilla-Moffett et al., 2016). IRGs and GBPs are dynamin-like

GTPases that are targeted to the membrane of cytoplasmic vacuoles containing bacteria, protists, or fungi (da Fonseca Ferreira-da-Silva et al., 2014; Pilla-Moffett et al., 2016). The targeted membranes are vesiculated, which leads to eventual rupture of the vacuoles and ultimately the death of exposed pathogens (Hunter and Sibley, 2012). Unexpectedly, *Atg5* was required for targeting the IRGs and GBPs to the PVM of *T. gondii* (Selleck et al., 2013; Zhao et al., 2008). We further found that only the LC3 conjugation system of autophagy but not lysosomal degradation is required to target these immune effectors to the PVM of *T. gondii* (Choi et al., 2014). Consequently, control of *T. gondii* infections by IFNG *in vitro* and *in vivo* depends on the LC3 conjugation system (Choi et al., 2014; Haldar et al., 2014; Ohshima et al., 2014). Furthermore, we found that the LC3 conjugation system is necessary and sufficient to target the IFN-inducible GTPases to membranes; upon relocation of the LC3 conjugation system to the plasma membrane or the mitochondria outer membrane, IRGs and GBPs were redirected to these endomembranes (Park et al., 2016).

Based on this similar genetic requirement for IFNG to function against the membranous structures of MNV and *T. gondii*, we speculated that the same effector mechanism of the IFN-inducible GTPases might be used by IFNG to inhibit the MNV RC. Here we show that the MNV RC was indeed marked with LC3 and targeted by the IFN-inducible GTPases upon their induction by IFNG. Consequently, the LC3 conjugation system and the IFN-inducible GTPases were required for IFNG to inhibit MNV replication in both mice and humans. These data suggest that IFNG inhibits the replication of +RNA viruses via LC3 dependent targeting of IFN-inducible GTPases to the RC. Moreover, it implies that IFNG utilizes the same effector mechanism to inhibit various pathogens replicating in cytosolic membranous shelters, including +RNA viruses as well as bacteria, protists, and fungi.

RESULTS

The LC3 Conjugation System of Autophagy Is Required for IFNG to Inhibit MNV Replication

Pharmacological modulation of canonical autophagy or lysosomal degradation has no substantial effect on the IFNG-mediated inhibition of MNV replication (Hwang et al., 2012). To genetically define the role of the canonical autophagy pathway in this antiviral activity of IFNG, we examined *Ulk* (uncoordinated 51-like kinase) and *Atg14*. ULK1 and ULK2 are serine/threonine-protein kinases of the autophagy initiation complex that induces autophagy upon various signals (Chan et al., 2007). ATG14 is an essential component of the phosphatidylinositol 3-kinase (PI3K) complex that nucleates the formation of isolation membrane (Diao et al., 2015). In primary bone marrow derived macrophages (BMDMs) from $Ulk1^{-/-}$, $Ulk2^{-/-}$, or littermate control mice, there was no significant difference in viral replication or inhibition by IFNG (Figure 1A). To rule out the possibility of phenotype masking due to the redundancy of *Ulk1* and *Ulk2*, we also tested mouse embryonic fibroblasts (MEFs) from $Ulk1^{-/-}Ulk2^{-/-}$ mice (McAlpine et al., 2013). To overcome the barrier of entry, the limiting step in infection (Orchard et al., 2016), transfection of MNV viral RNA (vRNA) is frequently used to analyze MNV replication in non-infectable cell types (Hwang et al., 2014). Upon transfection of MNV vRNA into $Ulk1^{-/-}Ulk2^{-/-}$ and control MEFs, infectious MNV were produced and inhibited by IFNG comparably in both

cell lines (Figures 1B and 1C). Similarly, MNV replication in control (*Atg14*$^{flox/flox}$) and *Atg14*-deficient (*Atg14*$^{flox/flox}$+*LysMcre*) BMDMs was comparable and similarly inhibited by IFNG (Figures 1D and 1E). These data affirmed our previous findings that the antiviral activity of IFNG requires a specific function of the ATG12-ATG5-ATG16L1 complex rather than the canonical autophagy pathway (Hwang et al., 2012).

Thus far, the only known function of the ATG12-ATG5-ATG16L1 complex is its E3-like ligase function to conjugate LC3 homologs to PE (Noda and Inagaki, 2015). LC3 conjugation also requires the proteolytic processing of LC3 by ATG4; we had previously ruled out a role of ATG4B, the major isoform of ATG4, in the IFNG-mediated control of MNV replication (Hwang et al., 2012). This suggested an LC3-conjugation independent function of the ATG12-ATG5-ATG16L1 complex, but the existence of other ATG4 isoforms undermined such a conclusion. In order to definitively examine the necessity of LC3 conjugation, we investigated the role of E2-like ATG3 in the IFNG-mediated inhibition of MNV replication. MNV replication was considerably less inhibited by IFNG in the *Atg3*-deficient (*Atg3*$^{flox/flox}$+*LysMcre*) BMDMs compared to the control (*Atg3*$^{flox/flox}$) (Figure 1F). Since LC3 was still substantially conjugated to PE due to suboptimal deletion of *Atg3* (Figure 1G), we further examined *Atg3*-deficient MEFs (*Atg3*$^{-/-}$) (Choi et al., 2014). We confirmed functional knock-out of ATG3 and consequent obstruction of autophagy in *Atg3*$^{-/-}$ MEF, as manifested by lack of conversion of cytosolic LC3-I to membrane-bound LC3-II and accumulation of autophagy adaptor/cargo p62 (Figure 1H). MNV replication was not significantly controlled by IFNG in these *Atg3*$^{-/-}$ MEFs (Figure 1I), but lentiviral expression of ATG3 back into the *Atg3*$^{-/-}$ MEFs restored the control of MNV replication by IFNG (Figures 1H and 1I). Collectively, these data show that the IFNG-mediated inhibition of MNV replication requires the E2-like ATG3 as well as the E1-like ATG7 and the E3-like ATG12-ATG5-ATG16L1 complex (Hwang et al., 2012).

The requirement of the entire LC3 conjugation system for IFNG to inhibit MNV replication further suggested that the LC3 homologs might be involved in such control. Although we previously did not observe any significant role of LC3B (Hwang et al., 2012), the existence of multiple LC3 homologs (i.e. LC3A, LC3B, gamma-aminobutyric acid type A receptor-associated protein (GABARAP), GABARAP-like 1 (GABARAPL1), and GABARAPL2 in the murine system) suggests a potential functional compensation among the homologs. In fact, we recently found that LC3 homologs fulfill redundant functions in the IFNG-mediated control of *T. gondii*; only with the knock-out/down of all LC3 homologs is the IFNG-mediated control of *T. gondii* lost (Park et al., 2016). Thus, to test the role of all LC3 homologs, we used the clustered regularly interspaced short palindromic repeat (CRISPR)/Cas9 system to knockout all remaining LC3 homologs, except one allele of *Gabarap*, in *Lc3b*$^{-/-}$ MEFs (Hwang et al., 2012) (Figures S1A and S1B). In the resultant MEFs and intermediate MEFs with wild type *Lc3a*, MNV replication was significantly less inhibited by IFNG, proportional to the knock-out of the LC3 homologs (Figure 1J). Collectively, these data demonstrated that LC3 homologs as well as the LC3 conjugation system were necessary for IFNG to inhibit MNV replication.

IFN-Inducible GTPases Are Targeted to the MNV RC via the LC3 Conjugation System

The parallel requirements of the LC3 conjugation system and the LC3 homologs in control of both MNV and *T. gondii* led us to speculate that the IFN-inducible GTPases might also be targeted by the LC3 conjugation system to the RC of MNV as they are targeted to the PVM of *T. gondii* (Park et al., 2016). In fact, LC3 localized on the MNV RC without IFNG activation (Figure S2A) in an *Atg5*-dependent manner (Figure S2B) and the localization of LC3 to the MNV RC requires the conjugation capability of LC3 (Figure S2C), just as it localizes on the PVM of *T. gondii* (Choi et al., 2016; Park et al., 2016). Thus, we further examined the potential targeting of IFN-inducible GTPases, IRGs and GBPs to the MNV RC. Because we cannot detect MNV RCs in cells pre-activated with IFNG (Hwang et al., 2012), we delayed IFNG treatment to allow MNV to form detectable RCs before being counteracted by IFNG. At 10–12 hours of MNV infection and simultaneous IFNG treatment, we detected formation of MNV RCs as well as expression of IFN-inducible GTPases (Figures 2 and S2D). Under these experimental conditions, both LC3 and IRGA6 (a representative effector of the IRG protein family) localized to a portion of the RCs (Figures 2A and 2B); we reasoned that such colocalization might be limited and transient due to inhibition of the RC by the recruited IFN-inducible GTPases. In a similar experimental condition, we also confirmed the localization of LC3 and IRGA6 to the RC of another +RNA virus, encephalomyocarditis virus (EMCV) (Figures S2E and S2F).

Although IFNG treatment and/or MNV infection did not substantially affect the total conjugation level of LC3 (Figure S3A), the localization of LC3 onto the MNV RC was enhanced upon IFNG activation (Figure S3B), reminiscent of the events that happened on the PVM of *T. gondii* (Park et al., 2016). Importantly, both LC3 and IRGA6 localization to the MNV RC were dependent on the functional LC3 conjugation system, as their localizations were substantially reduced upon *Atg5* deletion (Figures 2A and 2B). In contrast, the deletion of *Atg14*, which does not disturb LC3 conjugation (Choi et al., 2014), did not affect their localizations to the MNV RC (Figures 2C and 2D). These data demonstrated that both LC3 and the IFN-inducible GTPases were indeed recruited to the MNV RC, dependent on the functional LC3 conjugation system but independent of the canonical autophagy pathway.

Compared to the cooperative targeting and overlapping function of effector IRGs on target membranes, individual GBPs can stimulate distinct defense mechanisms (Pilla-Moffett et al., 2016). To identify specific GBPs associated with the MNV RC, we expressed individual epitope-tagged GBPs (GBP1, -2, -3, -5, and -7; deleted in $Gbp^{chr3-/-}$ mouse as described below) in both WT and $Gbp^{chr3-/-}$ BMDMs via lentiviral transduction. Only GBP1 and GBP2 significantly localized to the MNV RC upon IFNG activation in WT BMDMs (Figures 2E and 2F), but GBP2 was the only one that localized to the MNV RC in the absence of the other GBPs (Figures S3C and S3D). Interestingly, even GBP2 did not localize to the RC in the absence of IFNG activation (Figure S3E), suggesting that correct targeting requires an IFN-inducible co-factor(s) (e.g. a functional IRG system as described below). Like the effector IRGs, the localization of GBP2 to the MNV RC was dependent on *Atg5* but not on *Atg14* (Figures S4A-E). The IFN-inducible GTPases are known to be targeted only to vacuoles containing bacteria, protists, or fungi (da Fonseca Ferreira-da-Silva et al.,

2014; Pilla-Moffett et al., 2016). The data shown here establishes the membranous RCs of +RNA viruses, MNV and EMCV, as a destination of these IFN-inducible GTPases.

LC3 and IFN-Inducible GTPases Localize on the Membrane of the MNV RC

To examine the recruitment of IRGs and GBPs to the MNV RC at an ultrastructural level, we performed electron microscopy (EM) of the MNV RC. To ensure a high infection rate for efficient EM analysis, we utilized the BV-2 cell line (Hwang et al., 2014). We first confirmed that a representative IRG (i.e. IRGA6) and GBPs (using a pan-GBP antibody detecting GBP1, -2, -3, -4, -5) localized to the MNV RC upon the simultaneous MNV infection and IFNG treatment in BV-2 cells (Figure S4F). Under the same experimental condition, EM analysis revealed abundant vesicular structures around the nucleus only in MNV-infected cells (Figure 3A). We further found anti-ProPol (detecting both protease and polymerase of MNV) staining in these vesiculated areas (Figure 3B). Most anti-ProPol staining was associated with membranes and was significantly detectable only in infected cells (Figure 3B), suggesting that the vesicular structures are the MNV RC. Anti-LC3 staining was also detected around these anti-ProPol-positive structures in both untreated and IFNG-treated conditions (Figure 3B). Although simultaneous activation of the cells with IFNG did not significantly affect these structures, we detected both anti-IRGA6 and anti-GBP1-5 stainings on the vesicle membranes around anti-ProPol-positive structures in IFNG-treated cells (Figures 3C and 3D). While we could not definitively conclude the 3D topology of the proteins through these images, the majority of LC3, IRGA6, and GBP1-5 localized on the inner side of these vacuole-like structures together with ProPol, which is topologically the cytoplasmic side of the RC. These data suggest that LC3 and the IFN-inducible GTPases are recruited onto the cytoplasmic face of the MNV RC membrane and may exert their antiviral effect directly onto the membrane structure of the MNV RC.

IFNG Requires the IFN-Inducible GTPases to Inhibit MNV Replication *in vitro* and *in vivo*

To investigate the role of the IFN-inducible GTPases in the IFNG-mediated control of MNV, we obtained *Irgm1*$^{-/-}$*Irgm3*$^{-/-}$ mice (missing regulatory IRGs, *Irgm1 and Irgm3*; a non-functional IRG system) (Henry et al., 2009) and *Gbp* chromosome 3 deletion (*Gbp*$^{\text{chr3}-/-}$, with the deletion of *Gbp1, -2, -3, -5, -7*; a non-functional GBP system) mice (Yamamoto et al., 2012) (Figures S5A and S5B). MNV RC formation is inhibited in WT BMDMs pre-activated with IFNG, but not in *Atg5*-deficient BMDMs (Hwang et al., 2012) (Figure 4A). Similarly, MNV RC formation was not inhibited by IFNG in BMDMs lacking either a functional IRG or GBP system (Figures 4A and S5C). These data suggest that both IRGs and GBPs are required for IFNG to inhibit the MNV RC. We further investigated the control of MNV replication by IFNG in BMDMs from *Irgm1*$^{+/+}$*Irgm3*$^{+/+}$ *(WT)*, *Irgm1*$^{+/-}$*Irgm3*$^{+/-}$ *(HET)*, and *Irgm1*$^{-/-}$*Irgm3*$^{-/-}$ *(KO)* mice. In *Irgm1* and *Irgm3* WT and HET BMDMs, MNV replication was completely inhibited upon pre-activation of the cells with IFNG (Figure 4B). In KO BMDMs, however, MNV replication was not substantially controlled by IFNG. To confirm the specificity of the phenotype, we restored individual and dual expression of IRGM1 and IRGM3 in the KO BMDMs via lentiviral transduction and could restore the IFNG-mediated control of MNV replication in *Irgm1*$^{-/-}$*Irgm3*$^{-/-}$ BMDMs expressing IRGM3 at a functional level (Figures 4C and 4D). We further confirmed that MNV replication is controlled normally by IFNG in *Irgm1*$^{-/-}$ BMDMs (Figure S5D). In BMDMs

with *Gbp*^{chr3} deletion, MNV replication was substantially less inhibited by IFNG pre-treatment, compared to BMDMs with *Gbp*^{chr3} WT and HET (Figure 4E). When we restored the expression of GBP1 and GBP2 in *Gbp*$^{chr3-/-}$ BMDMs, only GBP2 was able to restore the IFNG-mediated control of MNV replication back to the level of WT BMDMs (Figures 4F and 4G). We further confirmed that MNV replication was substantially less inhibited by IFNG in *Gbp2*$^{-/-}$ BMDMs (Figure S6D). Although GBP2 did not localize onto the MNV RC in *Irgm1*$^{-/-}$*Irgm3*$^{-/-}$ BMDMs, IRGA6 localized onto the MNV RC in *Gbp*$^{chr3-/-}$ BMDMs (Figures S6A–C). These data corroborate a sequential recruitment model of the IFN-inducible GTPases onto their target membranes, i.e., IRGs prior to GBPs (Haldar et al., 2015), and further suggest a two-stage inhibitory mechanism of the GTPases against the MNV RC: the IRGs alone and in collaboration with the GBP system. Taken together, these data suggest that the IFN-inducible GTPases not only localize on the MNV RC but also play an antiviral role against MNV replication *in vitro*.

We previously showed that MNV infection in mice can be controlled by either type I or type II IFN signaling (Hwang et al., 2012). Although the IFN-inducible GTPases can be induced by both types of IFNs (Degrandi et al., 2007; Sorace et al., 1995), IRGs and GBPs are required for IFNG but not for type I IFNs to inhibit MNV replication *in vitro* (Figure S6E). In order to definitively show the crucial role of the LC3 conjugation system (i.e. *Atg5*) in type II IFNG mediated control of MNV infection *in vivo*, the absence of type I IFN signaling is required (Hwang et al., 2012). Therefore, after breeding the *Irgm1*$^{-/-}$*Irgm3*$^{-/-}$ and *Gbp*$^{chr3-/-}$ mice to type I IFN receptor deficient mice (*Ifnar*$^{-/-}$), we examined the survival of MNV infected mice and MNV replication in various organs as previously reported (Hwang et al., 2012). The control mice were significantly susceptible to MNV infection, implying a key role of type I IFN signaling in controlling the *in vivo* infection of MNV (Figures 5A and 5C). Nevertheless, consistent with the *in vitro* BMDM data, the KO mice of IFN-inducible GTPases (*Ifnar*$^{-/-}$*Irgm1*$^{-/-}$*Irgm3*$^{-/-}$ and *Ifnar*$^{-/-}$*Gbp*$^{chr3-/-}$) were more susceptible to MNV infection than their littermate control mice (Figures 5A and 5C); there was also substantially more viral replication in infected organs from KO mice than in organs from control mice (Figures 5B and 5D). Collectively, these data corroborate the importance of both type I IFN and type II IFN signaling in controlling MNV infection *in vivo* (Hwang et al., 2012) and further demonstrate that both IRG and GBP systems play crucial roles in the IFNG-mediated control of MNV replication *in vivo* as well as *in vitro*.

The LC3 Conjugation System and IFN-Inducible GTPases Are Required for IFNG to Inhibit MNV Replication in the Human System

The LC3 conjugation system and GBPs are well conserved in both mice and humans. In contrast, the IRG protein family is smaller in humans, with only two proteins, IRGM and IRGC, identified (Bekpen et al., 2009). Previous work has shown that the LC3 conjugation system and the GBPs counteract pathogens in humans, although the functional mechanisms vary considerably (Al-Zeer et al., 2013; Johnston et al., 2016; Ohshima et al., 2014; Selleck et al., 2015). To examine the role of the LC3 conjugation system in controlling norovirus replication in human cells, we obtained HeLa cells with *Atg7* or *Atg16l1* knocked-out by the CRISPR/Cas9 system (Selleck et al., 2015). Consistent with our results in mouse macrophages, both LC3 and GBPs localized on the RC of MNV that resulted from the

expression of MNV non-structural proteins (Hwang et al., 2012) (Figure 6A); the HeLa cell clones without functional *Atg7* or *Atg16l1* (Figure 6B) had substantially decreased localizations of LC3 and GBPs on the RCs (Figure 6C). In contrast, we did not detect any sign of IRGM localization on the MNV RC (Figure S6F). Using the vRNA transfection system, we further confirmed that the LC3 conjugation system was required for IFNG to inhibit MNV replication in HeLa cells (Figure 6D). Comparably, in human HAP1 cells with *Atg16l1*$^{-/-}$ or *Gbp*$^{1-7-/-}$ (complete human GBP knock-out) (Ohshima et al., 2014), MNV replication was substantially less inhibited by IFNG than in the control cells (Figures 6E and 6F). Taken together, these data demonstrated that both the LC3 conjugation system and GBP system were required for IFNG to inhibit MNV replication in both humans and mice.

DISCUSSION

Viral RCs provide a shelter for +RNA viruses to efficiently replicate, yet if and how the host immune defense system counteracts these structures have been poorly understood. We previously discovered an antiviral activity of IFNG functioning against the RC of MNV, which requires a nondegradative function of the E3-like ligase ATG12-ATG5-ATG16L1 complex (Hwang et al., 2012). However, its functional mechanism and pertinent effector proteins were unknown (Maloney et al., 2012). Using the *T. gondii* model, we found that the E3-like ligase complex can determine the target membrane of the IRGs and GBPs (Choi et al., 2016; Park et al., 2016). Based on these similar genetic requirements, here we identify the IFN-inducible GTPases, IRGs and GBPs, as the immune effectors functioning against the RC of MNV. Our data demonstrate that the membranous replication compartment of +RNA viruses can be controlled by the same immune mechanism used to target vacuoles containing bacteria, protists, or fungi, suggesting a universal immune defense mechanism against multiple intracellular pathogens that lurk in endomembrane structures.

LC3 localizes on the RCs of many +RNA viruses (Jackson et al., 2005; Panyasrivanit et al., 2009; Prentice et al., 2004; Sir et al., 2012; Zhang et al., 2014). This can result from the viruses hijacking the autophagy machinery or simply using LC3 for their own benefit (Reggiori et al., 2010; Sharma et al., 2014). In fact, it was recently shown that MNV infection induces autophagy, leading to the localization of LC3 on the RC and facilitation of viral replication (O'Donnell et al., 2016). Regardless of LC3's potential proviral roles, LC3 could simultaneously play an antiviral function by recruiting the IFN-inducible GTPases to RCs as shown in this study. While IFNG requires *Atg5* to inhibit MNV replication, it can also act in the absence of *Atg5* to inhibit the replication of other +RNA viruses, such as EMCV, murine hepatitis virus, and West Nile virus (Hwang et al., 2012). This suggests that IFNG has an additional antiviral function independent of *Atg5*, and thus independent of the LC3 conjugation system and the IFN-inducible GTPases, to inhibit the replication of these viruses. Therefore, the crucial antiviral role of the IFN-inducible GTPases against the RC of other +RNA viruses may only be revealed in the absence of this '*Atg5*-independent' antiviral activity of IFNG.

The crucial role of IRGs and GBPs in controlling intracellular pathogens, especially those hiding within vacuole-like structures, are well documented (Pilla-Moffett et al., 2016). In recent years, GBPs have also been recognized for their role in regulating canonical and

noncanonical inflammasome activation (Pilla-Moffett et al., 2016). In contrast, an antiviral function of the IRGs and GBPs has been poorly understood. For instance, the resistance of mice to Ebola virus, herpes simplex virus, and murine cytomegalovirus (Collazo et al., 2001; Taylor et al., 2000) was unaffected despite knockout of a regulatory IRG, while human IRGM has even been suggested to play a proviral role for hepatitis C virus, measles virus, and human immune deficiency virus type 1 (HIV-1) (GrEgoire et al., 2011). Human GBPs have been reported to play antiviral roles against dengue virus, EMCV, vesicular stomatitis virus, and influenza virus, but the underlying mechanisms are unknown (Anderson et al., 1999; Nordmann et al., 2012; Pan et al., 2012). Overall, there has been no clear functional mechanism determined for any anti- or proviral activities of IRGs and GBPs, with the exception of the recent report of GBP5 targeting the HIV-1 envelope glycoprotein independent of its GTPase activity (Krapp et al., 2016). Given this, the data shown here presents the definitive antiviral mechanism of both IRGs and GBPs against viral RCs, reflecting their general function against vacuolar pathogens.

IRGs and GBPs are known to oligomerize in a GTP-dependent manner on the membrane of pathogen-containing vacuoles, leading to vesiculation and subsequent disruption of the vacuole structures (Pilla-Moffett et al., 2016). The consequent exposure of the resident pathogens to the host cytoplasm leads to inhibition of the pathogen replication, activation of cytosolic pathogen sensors, and/or subsequent death of the pathogens and/or the host cells (Pilla-Moffett et al., 2016). Similarly, IRGs and GBPs may disrupt the structural integrity of the MNV RC and trigger additional antiviral responses by the host. However, translating the previously proposed membranolytic mechanism of the GTPases to the MNV RC has a major caveat: the size of the MNV RC. The MNV RC is roughly the same size as vesicles (ca. 50–300 nm in diameter) created from the PVM of *T. gondii* (ca. 5 um in length) during the process of IRG and GBP-mediated vacuole disruption (Wobus et al., 2004; Zhao et al., 2008). Thus, the dimensions of the MNV RC may be too small to be vesiculated by the IFN-inducible GTPases. If the IRGs and GBPs behave similarly on the membranes of the MNV RC as they do on the PVM of *T. gondii*, they may deform the structure and subsequently inhibit the function of the MNV RC, for example inhibiting viral genome replication and transcription, rather than demolishing the structure. It is also possible that the GTPases may even block the formation of the MNV RC as well as disrupt the formed RCs. How the IRGs and GBPs exert their antiviral function against the MNV RC will be a subject of future mechanistic investigation.

It has been proposed that IRG targeting of vacuolar pathogens is limited to a select but disparate group, i.e., the protist *T. gondii*, the bacterium *Chlamydia trachomatis*, and the fungus *Encephalitozoon cuniculi* (da Fonseca Ferreira-da-Silva et al., 2014; Springer et al., 2013; Tiwari et al., 2009). It is suggested that the cytosolic face of these plasma membrane-derived vacuoles containing these target organisms may be distinct from host endomembrane-bound intracellular compartments, because the organisms enter host cells via non-endocytic/phagocytic mechanisms (da Fonseca Ferreira-da-Silva et al., 2014). Since MNV enters cells through a host endocytic process (Perry and Wobus, 2010) and its RC is known to be composed of membranes derived from the ER, Golgi, and endosome (Hyde et al., 2009), our study does not support this hypothesis. Independent of the mechanism of entry, the membrane structures may share common patterns allowing the IRG system to be

activated and targeted. The control of MNV by IFNG is dependent on *Atg5*, because the putative *Atg5*-independent antiviral activity of IFNG cannot control MNV (Hwang et al., 2012). Likewise, the control of the disparate group of pathogens by IFNG might be dependent on the IRG system also because this is the only effective immune mechanism against these intracellular parasites. Further work is necessary to determine if there are any common pathogen-associated molecular patterns among this group of pathogens controlled by IRGs and how the IRG system is activated on these vacuole structures (Choi et al., 2016).

In summary, our study demonstrates that the LC3-conjugation system of autophagy has evolved to target the RC of the +RNA virus which in turn recruits the IFN-inducible GTPases for the inhibition of the RC. This provides a unifying working model in which the same effector mechanism is used against diverse intracellular pathogens that replicate inside cytosolic membrane structures. Importantly, this system is conserved in humans with a smaller set of the IFN-inducible GTPases. Further studies will determine how the cell-autonomous immune system utilizes the LC3 conjugation system to detect and destroy the membranous shelters of pathogens.

STAR Methods

CONTACT FOR REAGENT AND RESOURCE SHARING

Further information and requests for resources and reagents should be directed to and will be fulfilled by the Lead Contact, Seungmin Hwang (shwang@bsd.uchicago.edu).

EXPERIMENTAL MODEL AND SUBJECT DETAILS

Mice—All mice used in this study were from a C57BL/6 background. In all experiments, control and experimental mice were 6–8 week old littermates of both genders. Littermates of the same sex were housed together regardless of genotype. The following mice, including littermate controls, were used for bone marrow extraction: *Atg3*$^{flox/flox}$*+/−LysMcre*, *Atg5*$^{flox/flox}$*+/−LysMcre*, *Atg14*$^{flox/flox}$*+/−LysMcre, Irgm1*$^{-/-}$*Irgm3*$^{-/-}$, and *Gbp*$^{chr3-/-}$. *Atg3*$^{flox/flox}$*+/−LysMcre* mice were derived from *Atg3*$^{flox/flox}$ mice that were provided by Dr. You-Wen He, Duke University, USA (Jia et al., 2011). *Atg5*$^{flox/flox}$*+/−LysMcre* mice were provided by Dr. Herbert W. Virgin, Washington University in St. Louis, USA (Hwang et al., 2012). *Atg14*$^{flox/flox}$*+/−LysMcre* mice were provided by Dr. Shizuo Akira, Osaka University, Japan. *Irgm1*$^{-/-}$*Irgm3*$^{-/-}$ mice were provided by Dr. Gregory Taylor, Duke University, USA (Henry et al., 2009). *Gbp*$^{chr3-/-}$ mice were provided by Dr. Masahiro Yamamoto, Osaka University, Japan (Yamamoto et al., 2012). The following mice, including littermate controls, were used for *in vivo* MNV infection: *Irgm1*$^{-/-}$*Irgm3*$^{-/-}$*Ifnar*$^{-/-}$ and *Gbp*$^{chr3-/-}$*Ifnar*$^{-/-}$. To generate these mice, either *Irgm1*$^{-/-}$*Irgm3*$^{-/-}$ or *Gbp*$^{chr3-/-}$ mice were crossed with *Ifnar*$^{-/-}$ mice. *Ifnar*$^{-/-}$ mice were provided by Dr. Herbert W. Virgin (Hwang et al., 2012). All mice were housed and bred at the University of Chicago under specific-pathogen-free conditions in a biosafety level 2 facility in accordance with federal and university guidelines. All experimental procedures were approved by the Animal Care and Use Committee of the University of Chicago. For *in vivo* MNV infection experiments, mice were assigned randomly to experimental groups and were housed by matching genotype and gender. The day after group assignment, the mice were transferred from the breeding facility

to the infection facility; both are specific-pathogen-free and biosafety level 2 facilities. One week after transfer, the mice were infected with MNV. Mice were excluded from an experiment if they were noticeably sick or significantly smaller or weighed less than littermates on the day of infection. All *in vivo* experiments were conducted at least three times.

Primary Cells—The primary cells utilized in this study were murine bone marrow derived macrophages (BMDMs). Bone marrows were isolated from the femurs and tibias of 6–8 week old mice of both genders listed above, and plated in non-tissue culture treated 10-cm dishes in 10 mls of BMDM media. On day 4, 10 mls of fresh BMDM media was added. On day 7, BMDMs were detached from the dish using ice-cold 0.02% EDTA in DPBS (Sigma-Aldrich, E8008), and seeded in tissue culture treated plates or on coverslips for subsequent experiments. Remaining D7 BMDMs were frozen in BMDM media containing 10 % DMSO and used later to set up replicate experiments if necessary. BMDMs were rested for three days after seeding, and used for experiments as described in METHOD DETAILS and figure legends. BMDMs of the following mice were prepared in Washington University in St. Louis, USA and brought to the University of Chicago: *Ulk1*$^{-/-}$, *Ulk2*$^{-/-}$ and *Irgm1*$^{-/-}$. *Ulk1*$^{-/-}$ and *Ulk2*$^{-/-}$ BMDMs were derived from the mice provided by Dr. Sharon Tooze, London Research Institute, U.K. (McAlpine et al., 2013). *Irgm1*$^{-/-}$ BMDMs were derived from the mice provided by Dr. Gregory Taylor, Duke University, USA (Henry et al., 2009). The composition of BMDM media was Dulbeco's Modified Eagle Medium (Mediatech, 10–013), 10% fetal bovine serum (Biowest, US1520), 5% horse serum (Life Technology, 16050), 1× MEM nonessential amino acids (Mediatech, 25-025-CI), 1 mM sodium pyruvate (Mediatech, 25-000-CI), 2 mM L-glutamine (Mediatech, 25-005-CI) and macrophage colony-stimulating factor (M-CSF). The source of the M-CSF was 10% CMG14-12 conditioned medium (Takeshita et al., 2000) for MNV infection, and 10% L929 conditioned media (Stanley et al., 1977) for EMCV infection. All BMDMs were cultured at 37°C in 5% CO_2.

Cell Lines—Male *Ulk1*$^{-/-}$*Ulk2*$^{-/-}$ and female *Atg3*$^{-/-}$ murine embryonic fibroblasts (MEFs) were provided by Dr. Sharon Tooze, London Research Institute, U.K. (McAlpine et al., 2013) and Dr. Masaaki Komatsu, Tokyo Metropolitan Institute of Medical Science, Japan (Sou et al., 2008), respectively. Female *Lc3b*$^{-/-}$ MEFs were used to generate the CRISPR-KO cell lines of LC3 homologs and derived from *Lc3b*$^{-/-}$ mice that were obtained from Dr. Marlene Rabinovitch, Stanford University, USA. (Cann et al., 2007). Female HeLa WT, *Atg7*$^{-/-}$, and *Atg16l1*$^{-/-}$ cells were previously described (Selleck et al., 2015) and provided by Drs. Herbert W. Virgin and Ramnik Xavier. Male HAP1 WT, *Atg16l1*$^{-/-}$, and *Gbp*$^{1-7\,-/-}$ cells were previously described (Ohshima et al., 2014) and provided by Dr. Masahiro Yamamoto. Female BV-2 cells were provided by Dr. Yuanan Lu, University of Hawaii at Manoa, USA (Cox et al., 2009) and used to titer infectious virus. Male RAW264.7 cells were provided by Dr. Herbert W. Virgin and used to titer infectious virus. Female 293T cells, obtained previously from Dr. Herbert W. Virgin, were used to produce lentivirus. All cell lines were cultured at 37°C in 5% CO_2 in standard media: Dulbeco's Modified Eagle Medium (Mediatech, 10–013), 10% fetal bovine serum (Biowest, US1520), 1× MEM nonessential amino acids (Mediatech, 25-025-CI), 10 mM HEPES (Mediatech, 25-060-CI),

and 100 U/ml each of penicillin and streptomycin (Mediatech, 30-002-CI). All experiments were conducted within no more than 5 passages upon thawing of cell stocks. Protein/gene deletion for mutant cells were confirmed by western blot, PCR and/or qPCR as indicated in METHOD DETAILS and figure legends.

Viruses—All MNV infections were conducted using the MNV-1.CW3 strain (Thackray et al., 2007). All EMCV infections were conducted using EMCV strain K which was obtained from Dr. Marco Colonna, Washington University in St. Louis, USA (Hwang et al., 2012). MNV-1.CW3 viruses were prepared from a CDNA clone containing the genome of MNV-1.CW3. 1×10^6 293T cells were seeded in 6-well plates and transfected with 4 ug of the MNV-1.CW3 plasmid for 48 hours to produce virus. MNV and EMCV were further amplified in BV-2 cells. Infected cells were incubated until the cells showed >90% cytopathic effect, usually for 48 hours. Infected cells were then frozen and thawed, and the cell lysates containing viral particles were centrifuged for 20 minutes at 3000 rpm to remove the cell debris. Supernatants were further centrifuged for 3 hours at 26,250 rpm at 4°C to produce a concentrated virus stock. The viral stocks were frozen in small aliquots, and the titers of the stocks were determined by $TCID_{50}$. All viral infections were conducted with a viral stock aliquot having undergone only one cycle of freeze and thaw.

METHOD DETAILS

Viral Infection and Viral RNA Transfection—Viral infections were performed as previously described (Hwang et al., 2012; Nice et al., 2012). 1×10^5 cells (BMDM, BV-2, and HAP1) or 2×10^4 cells (MEF and HeLa) were seeded per well in 24-well plates. At 24 hours after seeding, cells were treated with mouse or human IFNG (Peprotech, 315-05 or 12410-1) or mouse IFN Beta (PBL Assay Science, 12410-1) for the time and at the doses indicated in the figures. At the time of infection, the media of cell was replaced with inoculum containing viruses at the MOI indicated in figure legends, and cells were infected for 30 minutes at room temperature. After incubation, the viral inoculum was removed, and cells were washed twice with PBS followed by addition of fresh media. In the case of simultaneous IFNG treatment with MNV infection for immunofluorescence assays, IFNG was added along with fresh media after infection. Transfection of MNV viral RNA (vRNA) is frequently used to overcome the barrier of entry, the limiting step of MNV infection (Orchard et al., 2016) when analyzing MNV replication in non-infectable cell types (MEFs, HAP1, and HeLa cells) (Hwang et al., 2014). MNV vRNA was isolated from the concentrated MNV stocks using TRI reagent (Sigma-Aldrich, T9424) according to the manufacturer's instruction. The amount of vRNA indicated in figure legends was transfected to cells using Lipofectamine 2000 (Invitrogen, 11668) according to the manufacturer's instruction. The infected or transfected cells were harvested at the time indicated in figure legends by fixation with 2% formaldehyde (Ted Pella, 18505) in PBS for 10 minutes at room temperature (for flow cytometry and immunofluorescence assays), by freezing at negative 80 (for replication analysis by 50% Tissue Culture Infectious Dose [$TCID_{50}$] or Plaque Assay [PA]), or by lysis with protein sample buffer (for western blot).

MNV Replication Analysis *in vivo*—For *in vivo* MNV infections, 6–8 week old littermate mice of both genders were infected perorally with 1×10^5 PFU of MNV in 25 ul of

standard media. Mouse weight was recorded upon infection and monitored every 12 hours. For survival experiments, mice were euthanized and recorded as dead, according to an approved IACUC protocols for >30% weight loss or if they became significantly moribund. For tissue viral burden analysis, infected mice were euthanized at 3 days post infection and organs were harvested and analyzed as previously described (Hwang et al., 2012). Organs were collected in standard media, subjected to a freeze-and-thaw cycle, and then homogenized in a bead beater using 1.0 mm zirconia/silica beads (BioSpec Products, 11079110z). After debris was removed by centrifugation, MNV titers in the homogenates were measured by $TCID_{50}$. Survival experiments were conducted 3 times using total 10 males and 6 females of *Irgm1*$^{+/-}$*Irgm3*$^{+/-}$*Ifnar*$^{-/-}$, 13 males and 7 females of *Irgm1*$^{-/-}$*Irgm3*$^{-/-}$*Ifnar*$^{-/-}$, 15 males and 11 females of *G*bp$^{+/-}$*Ifnar*$^{-/-}$, and 14 males and 12 females of *Gbp*$^{-/-}$*Ifnar*$^{-/-}$ mice. The tissue viral burden experiments were conducted 3 times using total 15 males and 5 females of *Irgm1*$^{+/-}$*Irgm3*$^{+/-}$*Ifnar*$^{-/-}$, 9 males and 5 females of *Irgm1*$^{-/-}$*Irgm3*$^{-/-}$*Ifnar*$^{-/-}$, 9 males and 10 females of *G*bp$^{+/-}$*Ifnar*$^{-/-}$, and 9 males and 5 females of *Gbp*$^{-/-}$*Ifnar*$^{-/-}$ mice.

$TCID_{50}$ and Plaque Assay—To quantitate infectious MNV, the infected cells with media were harvested by freezing at negative 80 and the infected cells were lysed through a freeze-and-thaw cycle. For Plaque Assay, the lysates were 10-fold serially diluted in standard media and added to RAW264.7 in 6-well plates. The cells were incubated for one hour with constant rocking at room temperature, and then the inoculums were replaced with overlay media containing 1% methylcellulose (Sigma-Aldrich, M0387). After incubation for four days, the overlay media was discarded and the cells were stained with 1% crystal violet (Fisher Chemical, C581) solution containing 20% ethanol for plaque counting. The limit of detection was calculated as the least number of infectious unit that can be detected at the lowest dilution (Hwang et al., 2012). For $TCID_{50}$ assay, the viral lysates were 10-fold serially diluted in standard media and added to BV-2 cells seeded in 96-well plates. 8-wells were infected for each dilution and further incubated for 5 days. $TCID_{50}$ was calculated by determining the dilution factor needed to show cytopathic effect (CPE) in 4 out of 8 (50%) wells. The limit of detection was calculated as the amount of virus that cause CPE in 4 out of 8 wells at the lowest dilution.

Western Blot—Cells were left untreated, or treated with IFNG (Peprotech, 315-05) or IFNB (PBL Assay Science, 12410-1), and/or treated with chloroquine (Sigma-Aldrich, C6628, 50 μM**)** as indicated in the figures. Total cell lysates were harvested in the protein sample buffer (0.1 M Tris [pH 6.8], 4% SDS, 4 mM EDTA, 286 mM 2-mercaptoethanol, 3.2 M glycerol, 0.05% bromophenol blue) and proteins were resolved by SDS-PAGE. Proteins were then transferred onto PVDF membranes and probed with primary antibody diluted in PBS/0.1% TWEEN 20 (PBST) containing 5% skim milk for overnight at 4°C and secondary antibody diluted in PBST with 5% skim milk for 1 hour at room temperature, on a side-to-side rocker. After each antibody incubation, the membranes were washed with PBST for three times of ten-minute-cycle. Probed proteins were detected using ECL reagents on a ChemiDoc system with Image Lab software (Bio-Rad). All antibodies were probed by the method described above except for LC3a (Cell Signaling), which was probed in TBS/0.1% TWEEN 20 with 5% BSA according to the manufacturer's instruction. The following

antibodies were used: MNV ProPol (Hwang et al., 2012); IRGB6 from Dr. Jonathan Howard, University of Cologne (Martens et al., 2004); IRGM1 and IRGM3 from Dr. Gregory Taylor, Duke University; ATG7, ATG16L1, LC3B, and p62 (Sigma-Aldrich); ATG3 (MBL International); GBP1-5, GBP2, and Actin-HRP (Santa Cruz Biotechnology); HA (the Frank W. Fitch Monoclonal Antibody Facility, The University of Chicago); 2A (EMD Millipore); LC3A (Cell Signaling Technology); GABARAP (Abcam); HRP Goat anti-mouse and HRP Donkey anti-rabbit (BioLegend); and HRP Donkey anti-goat (Jackson ImmunoResearch).

Immunofluorescence Analysis—For immunofluorescence analysis, cells were seeded on coverslips in 24-well plates and then infected with MNV or transfected with a plasmid expressing MNV open reading frame 1 (ORF1) (Hwang et al., 2012) with or without treatment of IFNG as indicated in figure legends. Upon fixation with 2% formaldehyde (Ted Pella, 18505), cells were permeabilized with 0.05% Saponin (Acros, 41923) in PBS, and blocked and probed in PBS containing 0.05% Saponin and 5% normal donkey serum (Jackson ImmunoResearch, 017-000-121). Fixation, permeabilization and 2 rounds of blocking were conducted for 10 minutes each at room temperature, and staining with primary and secondary antibodies was conducted for 1 hour each at room temperature. Samples were washed 5 times with PBS/0.01% Saponin for 5 min after each antibody incubation. Nuclei were stained with Hoechst 33342 (Invitrogen, H1399). Coverslips were mounted on glass slides with ProLong Diamond Antifade Mountant (Invitrogen, P36961). The images were acquired using the EVOS FL Cell Imaging System or Olympus FV1000 Laser Scanning Confocal Microscope (Integrated Light Microscopy Core Facility, The University of Chicago). Images from each channel were merged using ImageJ/Fiji. Primary antibodies detecting the following proteins were used: MNV ProPol (Hwang et al., 2012); IRGA6 from Dr. Jonathan Howard, University of Cologne (Martens et al., 2004); FLAG (Sigma-Aldrich); LC3B (MBL International); GBP1-5 (Santa Cruz Biotechnology); HA (The Frank W. Fitch Monoclonal Antibody Facility, The University of Chicago); double-strand RNA (J2; SCICONS); and IRGM (Abcam). The following secondary antibodies were used: Alexa Fluor 488 Donkey anti-Guinea Pig, Alexa Fluor 647 Donkey anti-Guinea Pig and Alexa Fluor 488 Donkey anti-Rabbit (Jackson ImmunoResearch); DyLight 649-Donkey anti-Rabbit, Alexa Fluor 555 Donkey anti-Rabbit, DyLight 649 Goat anti-Mouse, Alexa Fluor 555 Goat anti-Mouse and DyLight 488 Goat anti-Mouse (BioLegend). To quantitate the localization of proteins on the viral RC, a minimum of 3 independent experiments were performed and at least 50 RC-positive cells were counted per each condition in each experiment.

Flow Cytometry—For flow cytometric analysis of MNV replication, infected cells were stained with anti-ProPol and analyzed with a BD LSRFortessa cell analyzer (Hwang et al., 2012). After fixation with PBS/2% formaldehyde, cells were permeabilized with PBS/0.2% TritionX-100. Cells were then blocked and probed in PBS/0.2% TritonX-100/1% normal goat serum/1% normal mouse serum with rabbit anti-ProPol (Hwang et al., 2012) and DyLight 649-Donkey anti-Rabbit (Biolegend) for one hour each at room temperature. After each antibody incubation, cells were washed with PBS/0.2% TritionX-100. Uninfected and

stained samples served as gating controls. Flow data were analyzed using FlowJo (FlowJo, LLC).

Quantitative PCR (qPCR)—Cells were lysed with TRI reagent (Sigma-Aldrich, T9424) and total RNA was extracted according to the manufacturer's instruction. CDNA was reverse transcribed from 1 ug of total RNA using IMPROM-II reverse transcriptase (Promega, A3803) with random hexamer according to the manufacturer's instruction. qPCR was conducted using SYBR-green reagents on an Applied Biosystems StepOnePlus Real-Time PCR system. The qPCR primers used in this study are shown in Table S1.

Knock-out of *Lc3* Homologs—CRISPR/Cas9 technique was applied to knock-out *Lc3* homologs according to the published protocol (Ran et al., 2013). px458 (#48138) and px459 (#48139) plasmids were obtained from Addgene and the guide RNA sequences as shown in Table S2 were cloned into the plasmids to delete genomic DNA between the two double-strand-breaks. Cells were transfected with the plasmids using Lipofectamine 2000. After 48 hours, transfected cells were enriched through one passage of puromycin (Sigma-Aldrich, P9620) treatment (3 ug/ml). Enriched cells were diluted and seeded in 96-well plates, aiming for 0.5 cell/well, and the monoclonal colonies of cells were picked at 7 days after the set-up and further amplified. Genomic DNAs were extracted from the amplified cells and screened for deletion by PCR. Positive colonies containing desired deletion were further verified through sequencing and western blot analysis for the targeted protein. A monoclonal cell line harboring a desired deletion of a targeted *Lc3* homolog were then subjected to the next round of knock out of another *Lc3* homolog until all *Lc3* homologs were deleted. The primers used to screen the deletion of targeted DNA (Fig S1A) are shown in Table S2.

Lentiviral Transduction—pHAGE-N-Flag-HA (pHNHF) (Behrends et al., 2010) lentiviral vectors were used to express genes of interest in BV-2 cells, *Atg5*$^{flox/flox+/-}$*LysMcre* BMDMs, *Atg14*$^{flox/flox+/-}$*LysMcre* BMDMs, *Irgm1/Irgm3* WT/KO BMDMs, *Atg3* WT/KO MEFs and *Gbp*^{chr3} WT/KO BMDMs. The pHNHF vector is a Gateway destination vector that expresses proteins of interest with N-terminal FLAG-HA-tag and allows for puromycin selection of transduced cells. Modified lentiviral vector, pCDH-MCS-T2A-copGFP-MSCV (C274) (System Biosciences, Mountain View, CA; CD523A-1) (Hwang et al., 2012), was used to produce lentivirus for transduction of *Irgm1/Irgm3* WT/KO BMDMs. The T2A sequence in C274 is an 18 amino acid sequence which allows simultaneous expression of the protein of interest and copGFP during translation through self-cleavage. It also leaves 2A tag at the C-terminus of the expressed protein. All lentiviruses were generated in 293T cells as previously described (Choi et al., 2014; Hwang et al., 2012). The lentiviral vectors were transfected with the packaging vector (psPAX2) and the pseudotyping vector (pMD2.G). At 12 hours-post-transfection, the media was replaced with fresh media for target cells. Lentivirus released in media was collected at 24, 36, and 48 hours-post-transfection and filtered through 0.45 μm syringe filters (Millipore, MA). For MEF and BV-2 transduction, the cells were incubated with lentivirus for 48 hours and then selected with 3 ug/ml of puromycin (Sigma-Aldrich, P9620) for 3 passages. For BMDM transduction, lentiviruses were added to bone marrows on the day 4 of differentiation. On day 5, lentiviruses were replaced with fresh ones and the differentiating bone marrows were

further incubated until the day 7. BMDMs transduced with pHNHF lentiviruses were then selected with 1 ug/ml of puromycin (Sigma-Aldrich, P9620) for three days. BMDMs transduced with C274 lentiviruses were analyzed for transduction efficiency based on copGFP expression. The transduced cells were seeded for the experiments described in figure legends and the expression of transduced genes were validated by western blot analysis.

Electron Microscopy—BV-2 cells were left uninfected or infected with MNV at MOI=25 and simultaneously left untreated or treated with 100 U/ml IFNG. At 10 hpi, the cells were fixed, processed, and examined as previously described (Selleck et al., 2015). For ultrastructural analyses, cells were fixed in 2% paraformaldehyde (Polysciences, 00380)/ 2.5% glutaraldehyde (Polysciences, 18426) in 100 mM sodium cacodylate buffer (Sigma-Aldrich, C0250), pH 7.2 for 1 hr at room temperature. Samples were washed in sodium cacodylate buffer and post-fixed in 1% osmium tetroxide (Polysciences, 0972A) for 1 hour. Samples were then rinsed extensively in dH_20 prior to *en bloc* staining with 1% aqueous uranyl acetate (Ted Pella, 19481) for 1 hour. Following several rinses in dH_20, samples were dehydrated in a graded series 30%, 50%, 70%, 90%, 95% ethanol for 20 minutes each. Samples were further dehydrated in three changes of 100% ethanol for 20 minutes each followed by two changes in propylene oxide (Ted Pella, 18601) for 30 minutes each. Samples were then infiltrated with 1:1 propylene oxide:Eponate 12 resin (Ted Pella, 18012) for 30 minutes followed by 1:3 propylene oxide:Eponate 12 resin overnight at room temperature. Samples were infiltrated with freshly made Eponate 12 resin for eight hours, and then polymerized in the resin at 70°C overnight. Sections of 95 nm were cut with a Leica Ultracut UCT ultramicrotome (Leica Microsystems), stained with 1% uranyl acetate for 30 min and 3% lead citrate (Ted Pella, 19314) for 5 min, and viewed on a JEOL 1200 EX transmission electron microscope (JEOL USA) equipped with an AMT 8 megapixel digital camera and AMT Image Capture Engine V602 software (Advanced Microscopy Techniques). For immunolocalization, cells were fixed in 4% paraformaldehyde/0.05% glutaraldehyde in 100 mM piperazine-N,N[prime]-bis(2-ethanesulfonic acid) (PIPES) (Sigma-Aldrich, P6757)/0.5 mM $MgCl_2$ (Sigma-Aldrich, M8266), pH 7.2 for 1 hour at 4°C. Samples were then embedded in 10% gelatin and infiltrated overnight with 2.3 M sucrose (Sigma-Aldrich, S9378)/20% polyvinyl pyrrolidone (Sigma, PVP10) in PIPES/$MgCl_2$ at 4°C. Samples were trimmed, frozen in liquid nitrogen, and sectioned with a cryo-ultramicrotome. Sections of 50 nm were blocked with 5% FBS and 5% normal goat serum for 30 min and subsequently incubated with the indicated primary antibodies for 1 hour, followed by secondary antibodies: donkey anti-guinea pig conjugated to 12 nm colloidal gold (Jackson ImmunoResearch, 706-205-148), donkey anti-mouse conjugated to 18 nm colloidal gold (Jackson ImmunoResearch, 715-215-150) and goat anti-rabbit conjugated to 18 nm colloidal gold (Jackson ImmunoResearch, 111-215-144) for 1 hour. Sections were washed in PIPES buffer followed by a water rinse, and stained with 0.3% uranyl acetate/2% methyl cellulose (Sigma, M6385) and analyzed by transmission electron microscopy. All labeling experiments were conducted in parallel with controls omitting the primary antibody. These controls were consistently negative at the concentration of colloidal gold conjugated secondary antibodies used in these studies. Primary antibodies detecting the following proteins were used: MNV ProPol (Hwang et al., 2012), IRGA6 from Dr. Jonathan Howard,

University of Cologne (Martens et al., 2004), GBP1-5 (Santa Cruz Biotechology), and LC3B (MBL International).

QUANTITATION AND STATISTICAL ANALYSIS

All data were analyzed with Prism software (GraphPad) using one-way analysis of variation (One-way ANOVA) with multiple comparisons (for multiple samples), Student's t-test (for two samples), or Log-rank (Mantel-Cox) test (for *in vivo* survival) as indicated in figure legends. No specific method was used to determine whether the data met assumptions of the statistical approach. Unless otherwise stated, all experiments were performed at least three times and the data were combined for presentation as mean ± SEM. All differences not specifically indicated as significant were not significant (n.s., $p>0.05$). Significant value was indicated as; *, $p<0.05$; **, $p<0.01$; ***, $p<0.001$; ****, $p<0.0001$. Statistical parameters, including the statistical tests used, value of N (also what N represents, if necessary), definition of center, and dispersion and precision measures, are reported in the Figures and Figure Legends.

Supplementary Material

Refer to Web version on PubMed Central for supplementary material.

Acknowledgments

We thank Drs. Herbert W. Virgin (Washington University School of Medicine in St. Louis), Thirumala-Devi Kanneganti (St. Jude Children's Research Hospital), and Feng Zhang (Broad Institute) for sharing valuable research reagents for this study. This work was supported by startup fund to S.H., and in part by the Brinson Foundation Junior Investigator Grant, Cancer Research Foundation, an Institutional Research Grant (IRG-58-004-53-IRG) from the American Cancer Society, the University of Chicago Digestive Diseases Research Core Center (NIDDK P30DK42086), the University of Chicago Comprehensive Cancer Center Support Grant (P30 CA14599), the Cancer Center Core facilities (DNA sequencing and genotyping, flow cytometry, integrated microscopy, and monoclonal antibody), and the National Center for Advancing Translational Sciences of the National Institutes of Health (UL1 TR000430). S.B.B. was supported (in part) by NIH T32 GM007183 and H.M.B. was supported (in part) by NIH T32 AI007090. B.T.M. was supported by NCI-NIH award F31CA177194-01. G.A.T. was supported by VA grant I01 BX002369.

References

Al-Zeer MA, Al-Younes HM, Lauster D, Lubad MA, Meyer TF. Autophagy restricts Chlamydia trachomatis growth in human macrophages via IFNG-inducible guanylate binding proteins. Autophagy. 2013; 9:50–62. [PubMed: 23086406]

Anderson SL, Carton JM, Lou J, Xing L, Rubin BY. Interferon-induced guanylate binding protein-1 (GBP-1) mediates an antiviral effect against vesicular stomatitis virus and encephalomyocarditis virus. Virology. 1999; 256:8–14. [PubMed: 10087221]

Behrends C, Sowa ME, Gygi SP, Harper JW. Network organization of the human autophagy system. Nature. 2010; 466:68–76. [PubMed: 20562859]

Bekpen C, Marques-Bonet T, Alkan C, Antonacci F, Leogrande MB, Ventura M, Kidd JM, Siswara P, Howard JC, Eichler EE. Death and Resurrection of the Human IRGM Gene. PLoS Genet. 2009; 5:e1000403. [PubMed: 19266026]

den Boon JA, Diaz A, Ahlquist P. Cytoplasmic viral replication complexes. Cell Host Microbe. 2010; 8:77–85. [PubMed: 20638644]

Cann GM, Guignabert C, Ying L, Deshpande N, Bekker JM, Wang L, Zhou B, Rabinovitch M. Developmental expression of LC3α and β: Absence of fibronectin or autophagy phenotype in LC3β knockout mice. Dev Dyn. 2007; 237:187–195.

Chan EYW, Kir S, Tooze SA. siRNA Screening of the Kinome Identifies ULK1 as a Multidomain Modulator of Autophagy. J Biol Chem. 2007; 282:25464–25474. [PubMed: 17595159]

Changotra H, Jia Y, Moore TN, Liu G, Kahan SM, Sosnovtsev SV, Karst SM. Type I and Type II Interferons Inhibit the Translation of Murine Norovirus Proteins. J Virol. 2009; 83:5683–5692. [PubMed: 19297466]

Choi J, Biering SB, Hwang S. Quo vadis? Interferon-inducible GTPases go to their target membranes via the LC3-conjugation system of autophagy. Small GTPases. 2016:1–9.

Choi J, Park S, Biering SB, Selleck E, Liu CY, Zhang X, Fujita N, Saitoh T, Akira S, Yoshimori T, et al. The parasitophorous vacuole membrane of Toxoplasma gondii is targeted for disruption by ubiquitin-like conjugation systems of autophagy. Immunity. 2014; 40:924–935. [PubMed: 24931121]

Collazo CM, Yap GS, Sempowski GD, Lusby KC, Tessarollo L, Vande Woude GF, Sher A, Taylor GA. Inactivation of LRG-47 and IRG-47 reveals a family of interferon gamma-inducible genes with essential, pathogen-specific roles in resistance to infection. J Exp Med. 2001; 194:181–188. [PubMed: 11457893]

Cox C, Cao S, Lu Y. Enhanced detection and study of murine norovirus-1 using a more efficient microglial cell line. Virol J. 2009; 6:196. [PubMed: 19903359]

da Fonseca Ferreira-da-Silva M, Springer-Frauenhoff HM, Bohne W, Howard JC. Identification of the microsporidian Encephalitozoon cuniculi as a new target of the IFNγ-inducible IRG resistance system. PLoS Pathog. 2014; 10:e1004449–e1004449. [PubMed: 25356593]

Degrandi D, Konermann C, Beuter-Gunia C, Kresse A, Würthner J, Kurig S, Beer S, Pfeffer K. Extensive characterization of IFN-induced GTPases mGBP1 to mGBP10 involved in host defense. J Immunol. 2007; 179:7729–7740. [PubMed: 18025219]

Diao J, Liu R, Rong Y, Zhao M, Zhang J, Lai Y, Zhou Q, Wilz LM, Li J, Vivona S, et al. ATG14 promotes membrane tethering and fusion of autophagosomes to endolysosomes. Nature. 2015; 520:563–566. [PubMed: 25686604]

GrEgoire IP, Richetta C, Meyniel-Schicklin L, Borel S, Pradezynski F, Diaz O, Deloire A, Azocar O, Baguet J, Le Breton M, et al. IRGM Is a Common Target of RNA Viruses that Subvert the Autophagy Network. PLoS Pathog. 2011; 7:e1002422. [PubMed: 22174682]

Haldar AK, Foltz C, Finethy R, Piro AS, Feeley EM, Pilla-Moffett DM, Komatsu M, Frickel EM, Coers J. Ubiquitin systems mark pathogen-containing vacuoles as targets for host defense by guanylate binding proteins. Proc Natl Acad Sci USA. 2015; 112:E5628–E5637. [PubMed: 26417105]

Haldar AK, Piro AS, Pilla DM, Yamamoto M, Coers J. The E2-Like Conjugation Enzyme Atg3 Promotes Binding of IRG and Gbp Proteins to Chlamydia- and Toxoplasma-Containing Vacuoles and Host Resistance. PLoS ONE. 2014; 9:e86684. [PubMed: 24466199]

Henry SC, Daniell XG, Burroughs AR, Indaram M, Howell DN, Coers J, Starnbach MN, Hunn JP, Howard JC, Feng CG, et al. Balance of Irgm protein activities determines IFN-gamma-induced host defense. Journal of Leukocyte Biology. 2009; 85:877–885. [PubMed: 19176402]

Hunter CA, Sibley LD. Modulation of innate immunity by Toxoplasma gondii virulence effectors. Nat Rev Microbiol. 2012; 10:766–778. [PubMed: 23070557]

Hwang S, Alhatlani B, Arias A, Caddy SL, Christodoulou C, Cunha JB, Emmott E, Gonzalez-Hernandez M, Kolawole A, Lu J, et al. Murine norovirus: propagation, quantification, and genetic manipulation. Curr Protoc Microbiol. 2014; 33:15K–161.

Hwang S, Maloney NS, Bruinsma MW, Goel G, Duan E, Zhang L, Shrestha B, Diamond MS, Dani A, Sosnovtsev SV, et al. Nondegradative role of Atg5-Atg12/ Atg16L1 autophagy protein complex in antiviral activity of interferon gamma. Cell Host Microbe. 2012; 11:397–409. [PubMed: 22520467]

Hyde JL, Sosnovtsev SV, Green KY, Wobus C, Virgin HW, Mackenzie JM. Mouse Norovirus Replication Is Associated with Virus-Induced Vesicle Clusters Originating from Membranes Derived from the Secretory Pathway. J Virol. 2009; 83:9709–9719. [PubMed: 19587041]

Jackson WT, Giddings TH, Taylor MP, Mulinyawe S, Rabinovitch M, Kopito RR, Kirkegaard K. Subversion of Cellular Autophagosomal Machinery by RNA Viruses. 2005; 3:e156.

Jia W, He YW. Temporal regulation of intracellular organelle homeostasis in T lymphocytes by autophagy. J Immunol. 2011; 186:5313–5322. [PubMed: 21421856]

Johnston AC, Piro A, Clough B, Siew M, Virreira Winter S, Coers J, Frickel EM. Human GBP1 does not localize to pathogen vacuoles but restricts Toxoplasma gondii. Cellular Microbiology. 2016; 18:1056–1064. [PubMed: 26874079]

Krapp C, Hotter D, Gawanbacht A, McLaren PJ, Kluge SF, Stürzel CM, Mack K, Reith E, Engelhart S, Ciuffi A, et al. Guanylate Binding Protein (GBP) 5 Is an Interferon- Inducible Inhibitor of HIV-1 Infectivity. Cell Host Microbe. 2016; 19:504–514. [PubMed: 26996307]

Levine B, Mizushima N, Virgin HW. Autophagy in immunity and inflammation. Nature. 2011; 469:323–335. [PubMed: 21248839]

Maloney NS, Thackray LB, Goel G, HWANG S, Duan E, Vachharajani P, Xavier R, Virgin HW. Essential Cell-Autonomous Role for Interferon (IFN) Regulatory Factor 1 in IFN- -Mediated Inhibition of Norovirus Replication in Macrophages. J Virol. 2012; 86:12655–12664. [PubMed: 22973039]

Martens S, Sabel K, Lange R, Uthaiah R, Wolf E, Howard JC. Mechanisms regulating the positioning of mouse p47 resistance GTPases LRG-47 and IIGP1 on cellular membranes: retargeting to plasma membrane induced by phagocytosis. J Immunol. 2004; 173:2594–2606. [PubMed: 15294976]

McAlpine F, Williamson LE, Tooze SA, Chan EYW. Regulation of nutrient-sensitive autophagy by uncoordinated 51-like kinases 1 and 2. Autophagy. 2013; 9:361–373. [PubMed: 23291478]

Neufeldt CJ, Joyce MA, Van Buuren N, Levin A, Kirkegaard K, Gale M Jr, Tyrrell DLJ, Wozniak RW. The Hepatitis C Virus-Induced Membranous Web and Associated Nuclear Transport Machinery Limit Access of Pattern Recognition Receptors to Viral Replication Sites. PLoS Pathog. 2016; 12:e1005428–e1005428. [PubMed: 26863439]

Nice TJ, Strong DW, McCune BT, Pohl CS, Virgin HW. A Single-Amino-Acid Change in Murine Norovirus NS1/2 Is Sufficient for Colonic Tropism and Persistence. J Virol. 2012; 87:327–334. [PubMed: 23077309]

Noda NN, Inagaki F. Mechanisms of Autophagy. Annu Rev Biophys. 2015; 44:101–122. [PubMed: 25747593]

Nordmann A, Wixler L, Boergeling Y, Wixler V, Ludwig S. A new splice variant of the human guanylate-binding protein 3 mediates anti-influenza activity through inhibition of viral transcription and replication. The FASEB Journal. 2012; 26:1290–1300. [PubMed: 22106366]

Ohshima J, Lee Y, Sasai M, Saitoh T, Su Ma J, Kamiyama N, Matsuura Y, Pann-Ghill S, Hayashi M, Ebisu S, et al. Role of mouse and human autophagy proteins in IFN-γ-induced cell-autonomous responses against Toxoplasma gondii. J Immunol. 2014; 192:3328–3335. [PubMed: 24563254]

O'Donnell TB, Hyde JL, Mintern JD, Mackenzie JM. Mouse Norovirus infection promotes autophagy induction to facilitate replication but prevents final autophagosome maturation. Virology. 2016; 492:130–139. [PubMed: 26922001]

Orchard RC, Wilen CB, Doench JG, Baldridge MT, McCune BT, Lee YCJ, Lee S, Pruett-Miller SM, Nelson CA, Fremont DH, et al. Discovery of a proteinaceous cellular receptor for a norovirus. Science. 2016; 353:933–936. [PubMed: 27540007]

Pan W, Zuo X, Feng T, Shi X, Dai J. Guanylate-binding protein 1 participates in cellular antiviral response to dengue virus. Virol J. 2012; 9:292–292. [PubMed: 23186538]

Panyasrivanit M, Khakpoor A, Wikan N, Smith DR. Co-localization of constituents of the dengue virus translation and replication machinery with amphisomes. J Gen Virol. 2009; 90:448–456. [PubMed: 19141455]

Park S, Choi J, Biering SB, Dominici E, Williams LE, Hwang S. Targeting by AutophaGy proteins (TAG): Targeting of IFNG-inducible GTPases to membranes by the LC3 conjugation system of autophagy. Autophagy. 2016; 12:1153–1167. [PubMed: 27172324]

Perry JW, Wobus CE. Endocytosis of murine norovirus 1 into murine macrophages is dependent on dynamin II and cholesterol. J Virol. 2010; 84:6163–6176. [PubMed: 20375172]

Pilla-Moffett D, Barber MF, Taylor GA, Coers J. Interferon-Inducible GTPases in Host Resistance, Inflammation and Disease. Journal of Molecular Biology. 2016; 428:3495–3513. [PubMed: 27181197]

Prentice E, McAuliffe J, Lu X, Subbarao K, Denison MR. Identification and characterization of severe acute respiratory syndrome coronavirus replicase proteins. J Virol. 2004; 78:9977–9986. [PubMed: 15331731]

Ran FA, Hsu PD, Wright J, Agarwala V, Scott DA, Zhang F. Genome engineering using the CRISPR-Cas9 system. Nat Protoc. 2013; 8:2281–2308. [PubMed: 24157548]

Reggiori F, Monastyrska I, Verheije MH, Calì T, Ulasli M, Bianchi S, Bernasconi R, de Haan CAM, Molinari M. Coronaviruses Hijack the LC3-I-Positive EDEMosomes, ER-Derived Vesicles Exporting Short-Lived ERAD Regulators, for Replication. Cell Host Microbe. 2010; 7:500–508. [PubMed: 20542253]

Selleck EM, Fentress SJ, Beatty WL, Degrandi D, Pfeffer K, Virgin HW, MacMicking JD, Sibley LD. Guanylate-binding Protein 1 (Gbp1) Contributes to Cell-autonomous Immunity against Toxoplasma gondii. PLoS Pathog. 2013; 9:e1003320. [PubMed: 23633952]

Selleck EM, Orchard RC, Lassen KG, Beatty WL, Xavier RJ, Levine B, Virgin HW, Sibley LD. A Noncanonical Autophagy Pathway Restricts Toxoplasma gondii Growth in a Strain-Specific Manner in IFN-γ-Activated Human Cells. mBio. 2015; 6:e01157–e01115. [PubMed: 26350966]

Sharma M, Bhattacharyya S, Nain M, Kaur M, Sood V, Gupta V, Khasa R, Abdin MZ, Vrati S, Kalia M. Japanese encephalitis virus replication is negatively regulated by autophagy and occurs on LC3-I- and EDEM1-containing membranes. Autophagy. 2014; 10:1637–1651. [PubMed: 25046112]

Shulla A, Randall G. (+) RNA virus replication compartments: a safe home for (most) viral replication. Current Opinion in Microbiology. 2016; 32:82–88. [PubMed: 27253151]

Sir D, Kuo CF, Tian Y, Liu HM, Huang EJ, Jung JU, Machida K, Ou JHJ. Replication of Hepatitis C Virus RNA on Autophagosomal Membranes. J Biol Chem. 2012; 287:18036–18043. [PubMed: 22496373]

Sorace JM, Johnson RJ, Howard DL, Drysdale BE. Identification of an endotoxin and IFN-inducible cDNA: possible identification of a novel protein family. Journal of Leukocyte Biology. 1995; 58:477–484. [PubMed: 7561525]

Sou YS, Waguri S, Iwata JI, Ueno T, Fujimura T, Hara T, Sawada N, Yamada A, Mizushima N, Uchiyama Y, et al. The Atg8 conjugation system is indispensable for proper development of autophagic isolation membranes in mice. Molecular Biology of the Cell. 2008; 19:4762–4775. [PubMed: 18768753]

Springer HM, Schramm M, Taylor GA, Howard JC. Irgm1 (LRG-47), a regulator of cell-autonomous immunity, does not localize to mycobacterial or listerial phagosomes in IFN-γ-induced mouse cells. J Immunol. 2013; 191:1765–1774. [PubMed: 23842753]

Stanley ER, Heard PM. Factors regulating macrophage production and growth. Purification and some properties of the colony stimulating factor from medium conditioned by mouse L cells Journal of Biological Chemistry. 1977; 252:4305–4312. [PubMed: 301140]

Takeshita S, Kaji K, Kudo A. Identification and Characterization of the New Osteoclast Progenitor with Macrophage Phenotypes Being Able to Differentiate into Mature Osteoclasts. J Bone Miner Res. 2000; 15:1477–1488. [PubMed: 10934646]

Taylor GA, Collazo CM, Yap GS, Nguyen K, Gregorio TA, Taylor LS, Eagleson B, Secrest L, Southon EA, Reid SW, et al. Pathogen-specific loss of host resistance in mice lacking the IFN-gamma-inducible gene IGTP. Proc Natl Acad Sci USA. 2000; 97:751–755. [PubMed: 10639151]

Thackray LB, Wobus CE, Chachu KA, Liu B, Alegre ER, Henderson KS, Kelley ST, Virgin HW 4th. Murine noroviruses comprising a single genogroup exhibit biological diversity despite limited sequence divergence. J Virol. 2007; 81:10460–10473. [PubMed: 17652401]

Tiwari S, Choi HP, Matsuzawa T, Pypaert M, MacMicking JD. Targeting of the GTPase Irgm1 to the phagosomal membrane via PtdIns(3,4)P2 and PtdIns(3,4,5)P3 promotes immunity to mycobacteria. Nat Immunol. 2009; 10:907–917. [PubMed: 19620982]

Wobus CE, Karst SM, Thackray LB, Chang KO, Sosnovtsev SV, Belliot G, Krug A, Mackenzie JM, Green KY, Virgin HW. Replication of Norovirus in Cell Culture Reveals a Tropism for Dendritic Cells and Macrophages. Plos Biol. 2004; 2:e432. [PubMed: 15562321]

Yamamoto M, Okuyama M, Ma JS, Kimura T, Kamiyama N, Saiga H, Ohshima J, Sasai M, Kayama H, Okamoto T, et al. A Cluster of Interferon-γ-Inducible p65 GTPases Plays a Critical Role in Host Defense against Toxoplasma gondii. Immunity. 2012; 37:302–313. [PubMed: 22795875]

Zhang Y, Li Z, Ge X, Guo X, Yang H. Autophagy promotes the replication of encephalomyocarditis virus in host cells. Autophagy. 2014; 7:613–628.

Zhao Z, Fux B, Goodwin M, Dunay IR, Strong D, Miller BC, Cadwell K, Delgado MA, Ponpuak M, Green KG, et al. Autophagosome-independent Essential Function for the Autophagy Protein Atg5 in Cellular Immunity to Intracellular Pathogens. Cell Host Microbe. 2008; 4:458–469. [PubMed: 18996346]

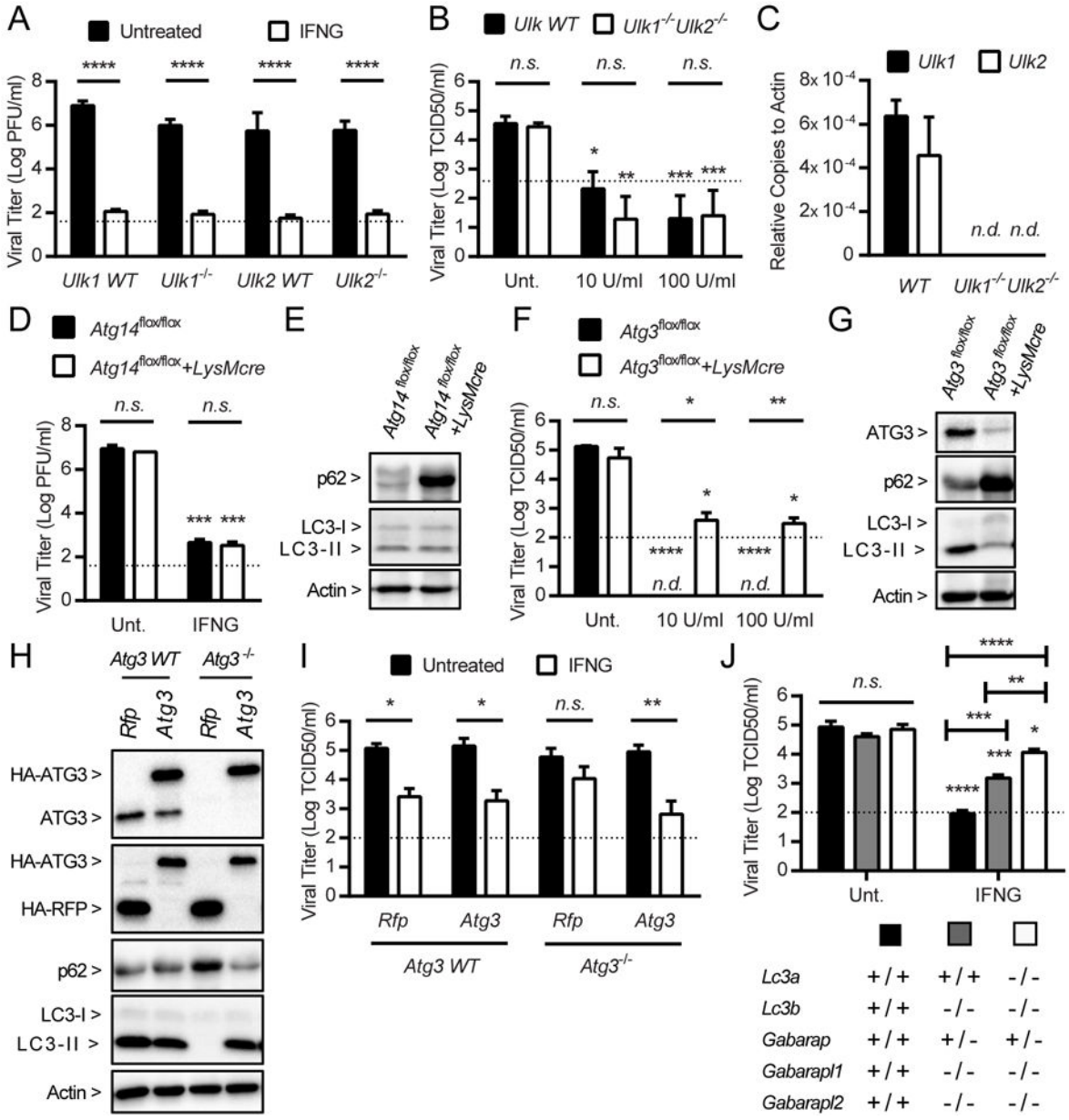

Figure 1. IFNG Inhibits MNV Replication via the LC3-Conjugation System of Autophagy

(A) Growth analysis of MNV in *Ulk1*$^{-/-}$, *Ulk2*$^{-/-}$ and WT BMDMs. Cells were untreated or treated with 100 U/ml IFNG for 12 hours and then infected with MNV at the multiplicity of infection (MOI) of 0.05. At 24 hour-post-infection (hpi), cells were harvested to titer infectious virus. N=5 replicates using 2 *Ulk1*$^{+/+}$ mice, 4 *Ulk1*$^{-/-}$ mice, 1 *Ulk2*$^{+/+}$ mouse, and 3 *Ulk2*$^{-/-}$ mouse. (B) Growth analysis of MNV in *Ulk1*$^{-/-}$*Ulk2*$^{-/-}$ and WT MEFs. Cells were treated with none (Unt.) or the indicated dose of IFNG for 24 hours and then transfected with 50 ng of MNV vRNA. At 24 hour-post-transfection (hpt), cells were harvested to titer infectious virus. N=5 replicates. (C) Quantitative PCR analysis for the transcript levels of *Ulk1* and *Ulk2* in *Ulk1*$^{-/-}$*Ulk2*$^{-/-}$ and WT MEFs. N=3 replicates. (D) Growth analysis of MNV in *Atg14*$^{flox/flox}$+*LysMcre* and littermate control *Atg14*$^{flox/flox}$

BMDMs as described in (A). N=3 replicates using 2 mice from each genotype. (E) A representative western blot of cells described in (D) on the level of p62 and the lipidation of LC3. Actin as loading control. N=3 replicates. (F) Growth analysis of MNV in *Atg3*$^{flox/flox}$+*LysMcre* and *Atg3*$^{flox/flox}$ BMDMs as described in (A). N=3 replicates using 2 mice from each genotype. (G) A representative western blot of cells described in (F), as described in (E). N=3 replicates. (H) A representative western blot of *Atg3*$^{-/-}$ and WT MEFs transduced with lentiviruses expressing *Atg3* WT or red fluorescent protein (RFP), as described in (E). N=3 replicates. (I) Growth analysis of MNV in the cells described in (H), as described in (B). N=3 replicates. (J) Growth analysis of MNV in the cells with deletions of *Lc3* homologs as indicated on the bottom, as described in (B). N=3 replicates. For all experiments with quantitative analysis, data are shown as mean ± SEM. One-way ANOVA with Tukey's multiple comparisons test; n.d., not detected. n.s., not significant; *, $p<0.05$; **, $p<0.01$; ***, $p<0.001$; ****, $p<0.0001$. Dashed line indicates the limit of detection. See also Figure S1.

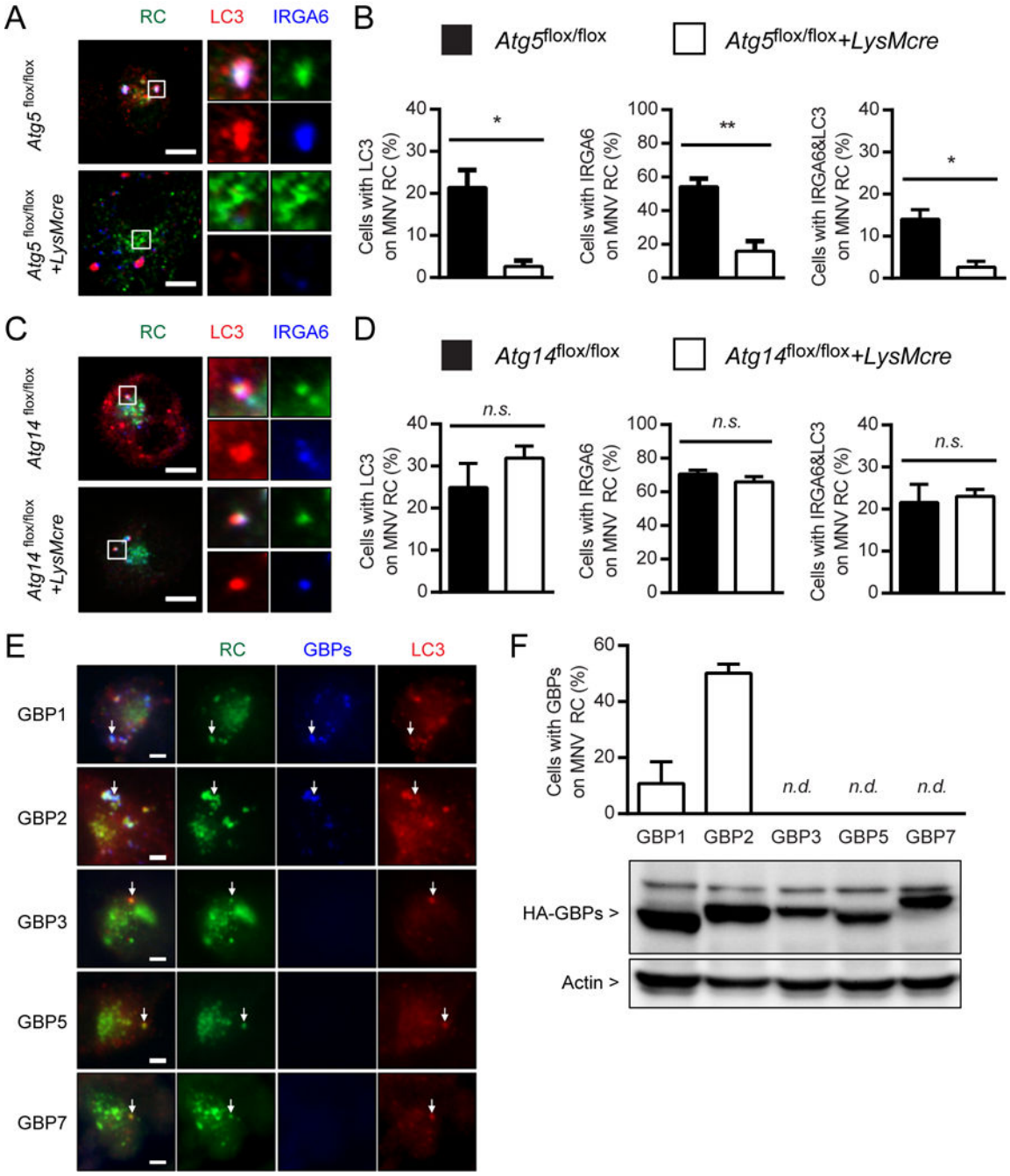

Figure 2. IFN-Inducible GTPases Are Targeted to the MNV RC via the LC3-Conjugation System

(A and B) Immunofluorescence assay for the localization of LC3 and IRGA6 with regard to the MNV RC (via anti-ProPol detecting both protease and polymerase of MNV) at 10 hpi in *Atg5*$^{flox/flox}$+*LysMcre* and *Atg5*$^{flox/flox}$ BMDMs upon MNV infection at MOI=5 and simultaneous 100 U/ml IFNG treatment. Representative images (A) and quantitation (B). Data as mean±SEM. N=3 replicates using 2 mice from each genotype. Student's t-test. *, $p<0.05$; **, $p<0.01$. Scale bars, 5 μm. (C and D) The same assays as described for (A) and (B) in *Atg14*$^{flox/flox}$+*LysMcre* and *Atg14*$^{flox/flox}$ BMDMs. Data as mean±SEM. N=3

replicates using 2 mice from each genotype. Student's t-test. n.s., not significant. (E and F) The same assays as described for (A) and (B) in WT BMDMs transduced with lentiviruses expressing the indicated GBPs. Individual FLAG/HA-tagged GBP was detected by anti-FLAG (E) or anti-HA (F, bottom panel) antibodies. White arrows in (E) indicate colocalization. n.d., not detected. A representative western blot in F for the expression of individual GBPs. N=3 replicates using 2 mice. See also Figures S2, S3, and S4.

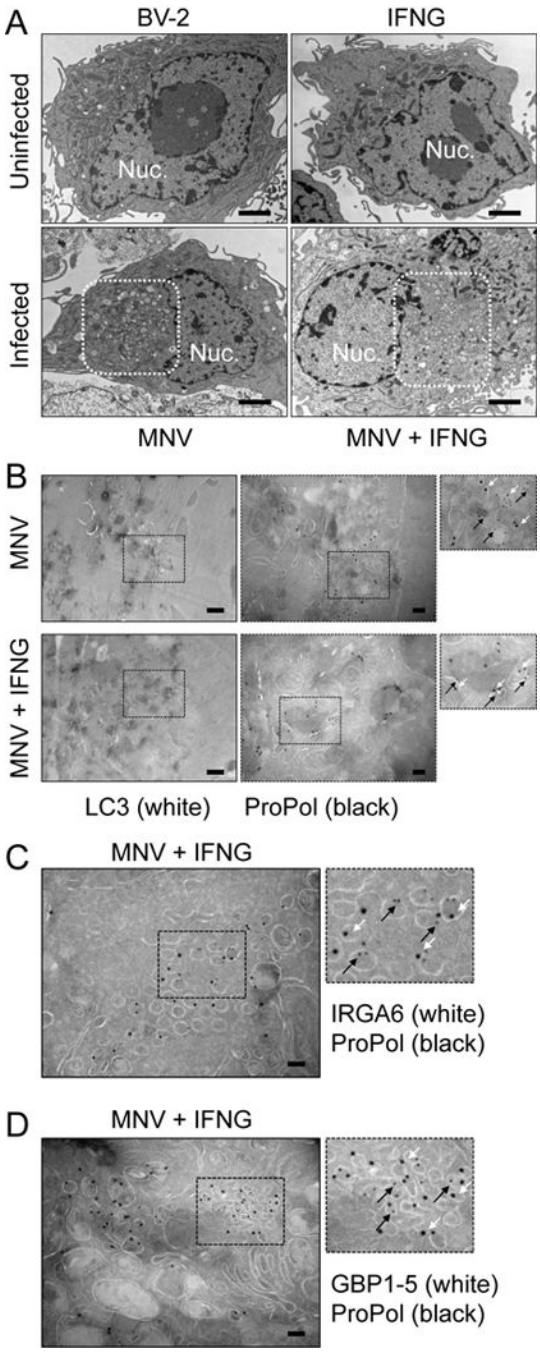

Figure 3. LC3 and IFN-Inducible GTPases Localize on the Membrane of the MNV RC

(A) Transmission electron microscopy of BV-2 cells: uninfected (BV-2), activated with 100 U/ml IFNG for 12 hours (IFNG), at 12 hpi of MNV infection at the MOI of 25 (MNV), and at 12 hpi of MNV infection after 12 hour activation with IFNG (MNV + IFNG). Scale bars, 2 μm. Dotted rectangles show the area of vacuole structures. N=2 replicates. (B) Cryo-immuno-EM localization of LC3 and ProPol in (MNV) and (MNV + IFNG) condition as described in (A). Scale bars, 500 nm (left) and 100 nm (center). (C and D) The same analysis as described in (B) for IRGA6 and ProPol (C) and GBP1-5 and ProPol (D). Scale

bars, 100 nm. White arrows indicate LC3 (B), IRGA6 (C), and GBP1-5 (D). Black arrows indicate ProPol. N=2 replicates. See also Figure S4.

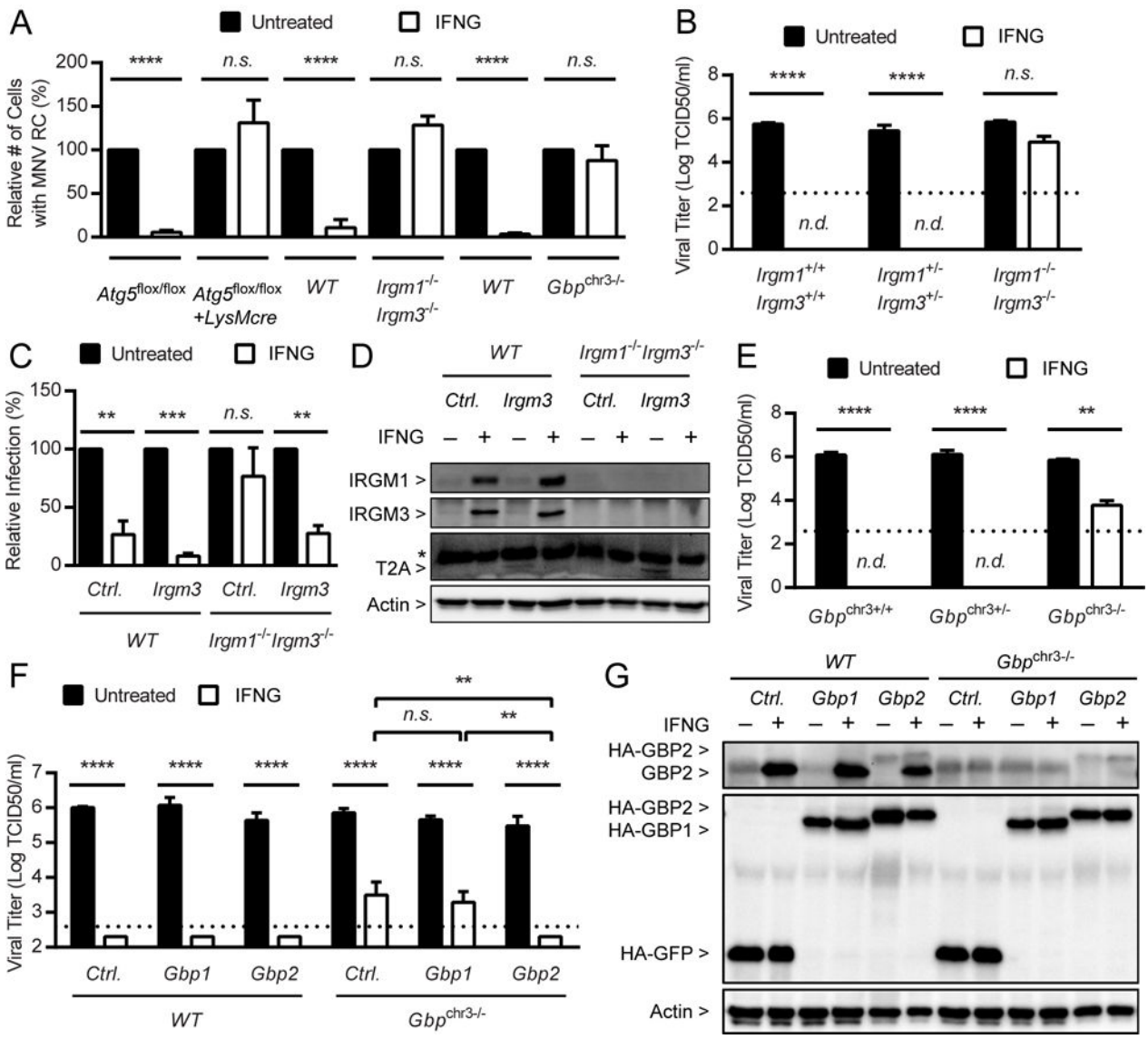

Figure 4. IFNG Requires the IFN-Inducible GTPases to Inhibit MNV Replication *in vitro*

(A) Quantitation of MNV RCs in BMDMs from *Atg5*$^{flox/flox}$+*LysMcre*, *Irgm1*$^{-/-}$*Irgm3*$^{-/-}$, *Gbp*$^{chr3-/-}$, and respective littermate control mice. Cells were either untreated or treated with 100 U/ml IFNG for 12 hours before infection with MNV at MOI=5 and harvested and analyzed at 12 hpi with anti-ProPol immunofluorescence. Data as mean±SEM. N=3 replicates using 2 mice for each genotype. Student's t-test. n.s., not significant; p<0.001; ****. (B) Growth analysis of MNV in *Irgm1*$^{-/-}$*Irgm3*$^{-/-}$ or control BMDMs. Cells were untreated or treated with 100 U/ml IFNG for 24 hours and then infected with MNV at MOI=0.05. At 24 hpi, cells were harvested to titer infectious virus. N=3 replicates using 2 mice for each genotype. (C) Growth analysis of MNV in *Irgm1*$^{-/-}$*Irgm3*$^{-/-}$ and control BMDMs transduced with lentiviruses expressing green fluorescent protein (GFP) (Ctrl.) or IRGM3. Cells were untreated or treated with 100 U/ml IFNG for 12 hours and then infected with MNV at MOI=5. At 12 hpi, cells were harvested to analyze viral replication with anti-ProPol flow cytometry. N=3 replicates using 2 mice for each genotype. (D) Representative

western blot data of cells described in (C) for the expression of IRGM1, IRGM3, and transduced IRGM3 (detected with anti-T2A antibody against remaining T2A at the C-term of IRGM3 expressed from lentivirus). * indicates non-specific signal. Actin as loading control. N=3 replicates. (E) Growth analysis of MNV in *Gbp*$^{chr3-/-}$ or control BMDMs as described in (B). N=5 replicates using 2 mice for each genotype. (F) Growth analysis of MNV in *Gbp*$^{chr3-/-}$ or control BMDMs transduced with lentiviruses expressing GFP (Ctrl.), GBP1 or GBP2 as described in (B). N=3 replicates using 2 mice for each genotype. (G) A representative western blot of cells described in (F) for the expression of IFN-induced endogenous GBP2 (as a representative) and transduced genes (HA-tagged). Actin as loading control. N=3 replicates. For (B), (C), (E), and (F), data as mean±SEM. One-way ANOVA with Tukey's multiple comparisons test; n.d., not detected. n.s., not significant; *, $p<0.05$; **, $p<0.01$; ***, $p<0.001$; ****, $p<0.0001$. Dashed line indicates the limit of detection. See also Figures S5 and S6.

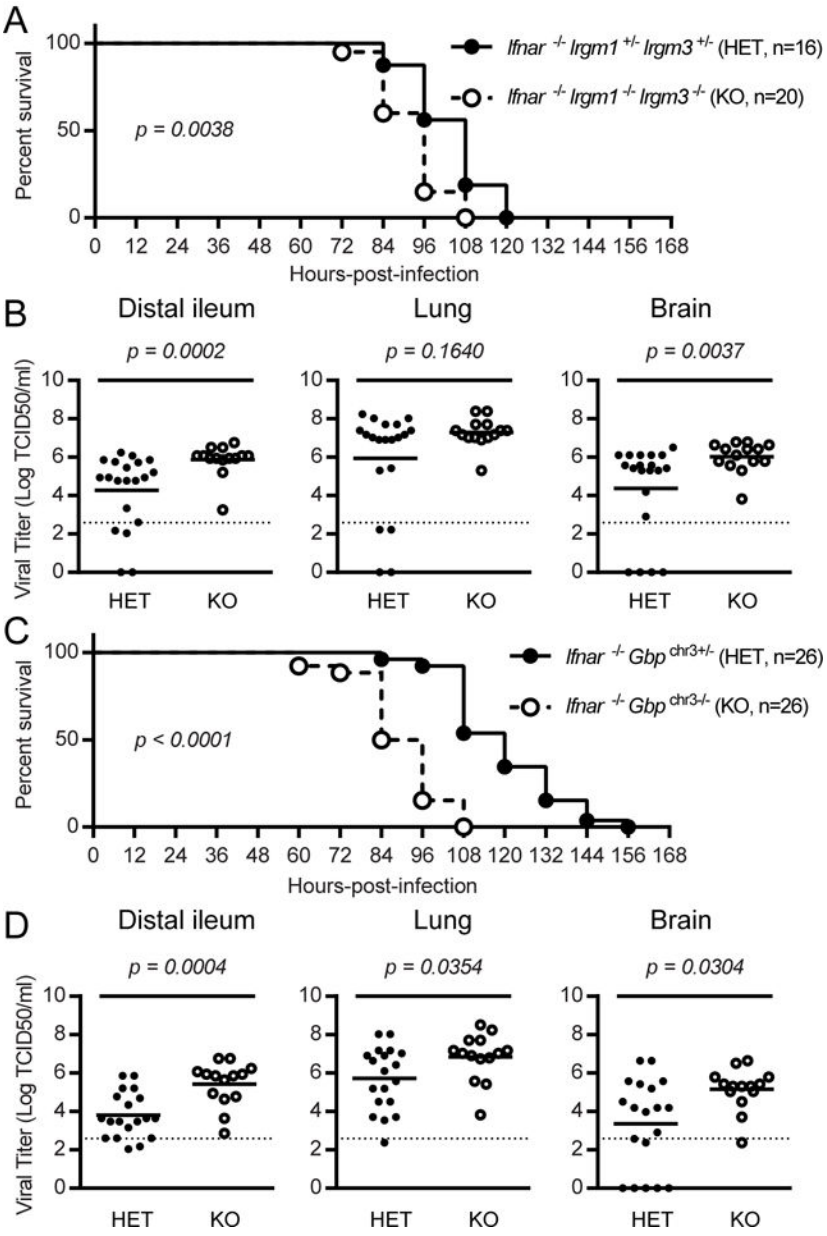

Figure 5. IFN-Inducible GTPases Are Required to Control MNV *in vivo*

(A) Survival of *Ifnar*$^{-/-}$*Irgm1*$^{+/-}$*Irgm3*$^{+/-}$ (HET) and *Ifnar*$^{-/-}$*Irgm1*$^{-/-}$*Irgm3*$^{-/-}$ (KO) mice after peroral infection with 1×10^5 plaque forming unit (PFU) of MNV. Numbers in parentheses indicate the number of mice used. (B) Tissue viral burden in the indicated organs of mice at 3 days-post-infection as described in (A). (C and D) The same analysis as described in (A) and (B) with *Ifnar*$^{-/-}$*Gbp*$^{\text{chr3}+/-}$ (HET) and *Ifnar*$^{-/-}$*Gbp*$^{\text{chr3}-/-}$ (KO) mice. (A) and (C) were analyzed using a Log-rank (Mantel-Cox) test and (B) and (D) were analyzed using a Student's t-test. p-values are indicated in the figure. See also Figure S6.

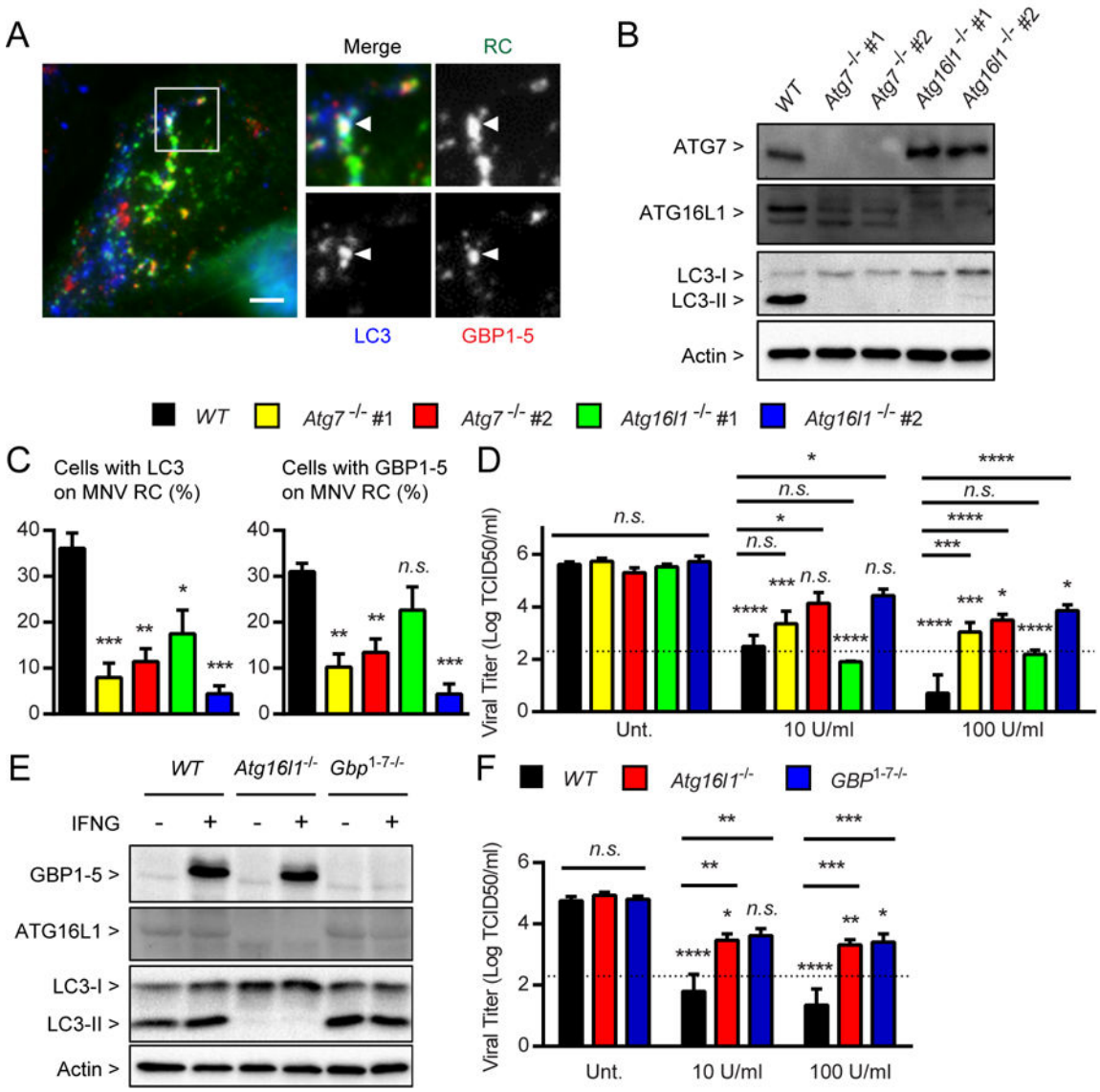

Figure 6. The LC3 Conjugation System and IFN-Inducible GTPases Are Required for IFNG to Inhibit MNV Replication in the Human System

(A) Immunofluorescence assay for the localization of LC3 (Blue) and GBP1-5 (Red) with regard to the MNV RC (Green) in HeLa cells transfected with a plasmid expressing MNV ORF1 for 6 hours followed by treatment with 100 U/ml IFNG for an additional 18 hours. Representative images shown here. White arrowheads indicate representative colocalization. Scale bar, 10 μm. N=3 replicates. (B) Representative western blot of HeLa cells; WT, two clones of *Atg7*$^{-/-}$, and two clones of *Atg16l1*$^{-/-}$. N=3 replicates. (C) Quantitation of immunofluorescence assay for the localization of LC3 (left) and GBP1-5 (right) with regard to the MNV RC as described in (A) for the cells described in (B). Data as mean±SEM. N=3 replicates. One-way ANOVA with Dunnett's multiple comparisons test; n.s., not significant; *, p<0.05; **, p<0.01; ***, p<0.001. (D) Growth analysis of MNV in the cells described in (B). The cells were treated with none (Unt.) or the indicated dose of IFNG for 24 hours and then transfected with 50 ng MNV viral RNA. At 24 hpt, cells were harvested to titer

infectious virus. N=3 replicates. (E) Representative western blot of HAP1 cells; WT, *Atg16l1*$^{-/-}$, and *Gbp*$^{1-7-/-}$. Cells were treated with none or 100 U/ml IFNG for 24 hours. N=3 replicates. (F) Growth analysis of MNV as described in (D) for the cells described in (E). N=3 replicates. Data as mean±SEM. (D) and (F) were analyzed using a One-way ANOVA with Tukey's multiple comparisons test; n.s., not significant; *, $p<0.05$; **, $p<0.01$; ***, $p<0.001$; ****, $p<0.0001$. Dashed line indicates the limit of detection. See also Figure S6.